AN ABSTRACT OF THE THESIS OF

Seung-Bae Kim for the degree of Master of Science in Electrical & Computer Engineering presented on July 11, 1988.

Title: Diamond-Like Carbon Films for Electroluminescent Applications.

Abstract approved: Redacted for privacy

Dr. John F. Wager

White electroluminescence (EL) was observed for the first time from diamond-like carbon (DLC) films at room temperature. Electroluminescence was observed by the application of ac voltages in excess of 200 V to a metal-insulator-semiconductor (i.e. DLC)-insulator-metal (MISIM) device structure.

For EL applications, three types of the DLC films were prepared by plasma-enhanced chemical vapor deposition (PECVD) using a commercially available reactor (Semi-Group System 1000). The plasma excitation frequency was either 13.56 MHz or 100 kHz and the system has a capacitively coupled, parallel plate configuration in which the substrate electrode was either grounded or powered. DLC films were deposited using a source gas mixture of 10 % methane diluted in helium.

The critical temperature for obtaining a DLC deposition was found to be a function of the electrode spacing. Using the conventional electrode spacing of 25 mm, it was not possible to deposit DLC films above 200° C. When the electrode spacing was decreased to 14.5 mm, however, DLC films were obtained at substrate temperatures up to 300° C.

The optical bandgap of the DLC films could be varied from 2.2-3.0 eV using typical process deposition parameters. In contrast to other reports, the optical bandgap did not strongly depend on the deposition temperature, rf power, or pressure. A reduction in optical bandgap of thermally annealed DLC films was observed, compared to that of the as-deposited DLC films.

The films also exhibited photoluminescence (PL) which was observed at room temperature. The EL and the PL spectra were compared. The PL peak energy shifts were observed by decreasing measuring temperature and by changing the deposition power. Periodic oscillations in the PL spectrum were observed when a low optical pumping energy was used; these oscillations were attributed to C-H wagging modes.

Diamond-Like Carbon Films for Electroluminescent Applications

by

Seung-Bae Kim

A THESIS

submitted to

Oregon State University

in partial fulfillment of
the requirements for the
degree of

Master of Science

Completed July 11, 1988

Commencement June 1989

APPROVED:

Redacted for privacy

Assistant Professor of Electrical & Computer Engineering

Redacted for privacy

Head of Department of Electrical & Computer Engineering

Redacted for privacy

Dean of Graduate School

Date thesis is presented July 11, 1988

Typed by Yoon-Sin Kim for Seung-Bae Kim

ACKNOWLEDGEMENTS

I would like to express my sincere gratitude to my advisor, Professor John F. Wager, for the support, guidance, and encouragement he has given me throughout this work, and to Professor J. A. Van Vechten for the idea of employing DLC as an EL material.

Special thanks to Professor S. J. T. Owen, Professor A. Wallace, Professor J. Gardner, and Dr. C. King for being on my graduate committee and for providing useful suggestions.

I also would like to thank Dr. C. King, Dr. D. Tunge, and J. Kollas of Planar Systems for supplying substrates and assisting with device characterization.

I indebted to T. W. Dobson, P. Kamdar, and R. C. McArthur for proofreading my thesis.

The financial support provided by the U. S. Army Electronics Technology and Devices Laboratory through a Scientific Services Agreement issued by Battelle and also by a grant from the Murdock Foundation is gratefully acknowledged.

To my parents and wife

TABLE OF CONTENTS

LIST OF FIGURES

LIST OF TABLES

Diamond-Like Carbon Films for Electroluminescent Applications

Chapter 1. Introduction

Display devices as interfaces between man and machine have played an important role in our information society. This role will continue in the foreseeable future which makes display device technology an important issue. Display devices can be classified by their operating modes: active mode (emits lights by itself) and passive mode (needs ambient light), as shown in Table 1.1.

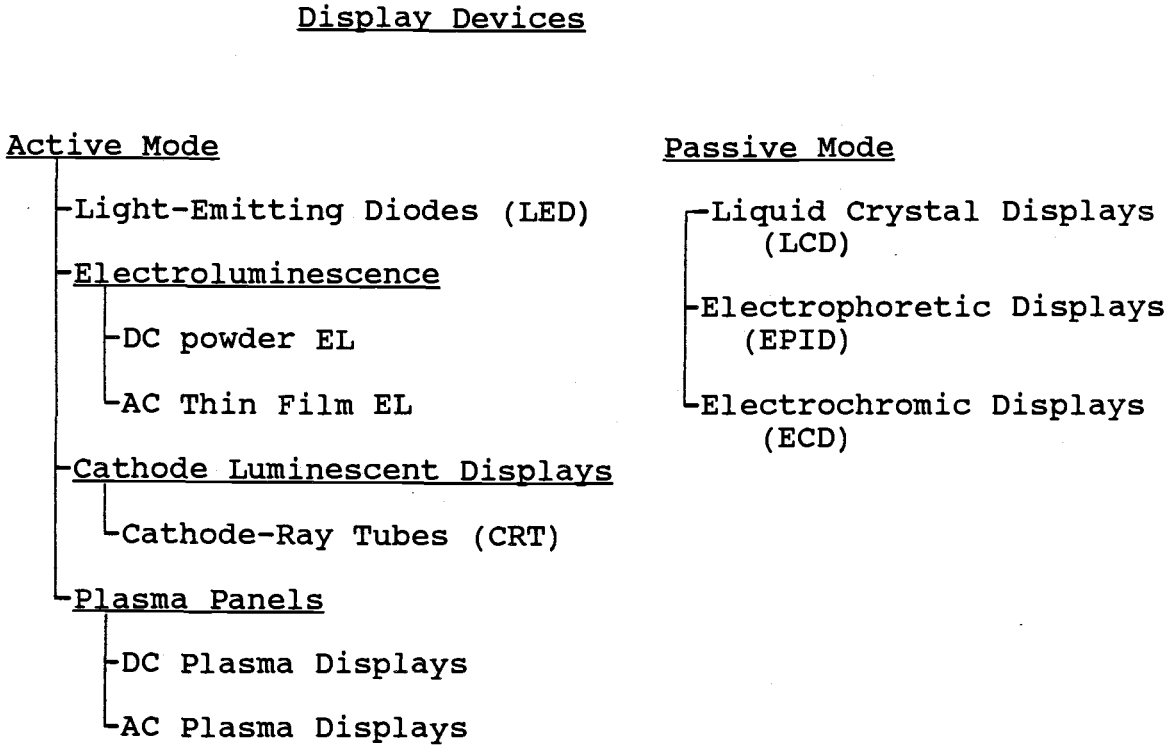

Table 1.1. Classification of display devices by their operating modes

In spite of its bulkiness and high power dissipation, the CRT has almost exclusively been used as an information display device due to its long operation lifetime, display contrast, brightness, and addressability. One of the biggest disadvantages of the CRT is the inherent problem of making a large screen. Alternative solutions to this problem have been proposed, such as electroluminescent (EL) panel displays.

As shown in Table 1.1, EL displays can be roughly classified [1] into dc powder electroluminescent and ac thin film electroluminescent (ACTFEL) display devices. A typical ACTFEL device structure is shown in Fig. 1.1, in which the

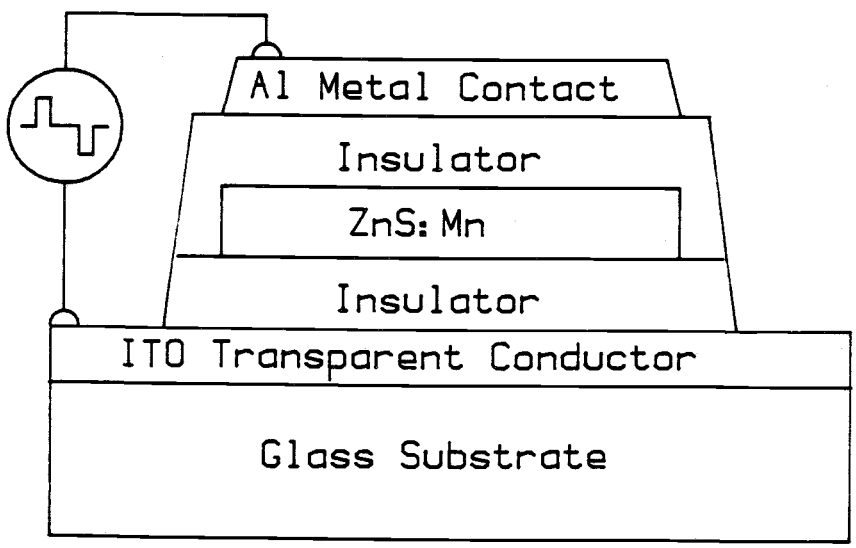

Figure 1.1. A structure of the typical ACTFEL device.

host material is a thin film of semiconductor, usually ZnS, containing a phosphorescent impurity, typically Mn. Since ACTFEL device performance depends strongly on the host material, most of the research has focused on ZnS and related II-VI semiconductors. In addition to the host material, the insulator [2] and driving waveform employed are also known to be important factors in ACTFEL device performance.

Diamond-like carbon (DLC) as an alternative host material for ACTFEL display applications is proposed in this thesis. DLC has similar properties to diamond, e.g. an abundance of sp^3 bonding, a relatively large bandgap, and high resistivity. Electroluminescence of diamond [3] has been known for a long time. Recently electroluminescence in natural and synthetic diamond has been reported elswhere [4-7].

1.1 Diamond-Like Carbon as an EL Material

It was reasoned that DLC could be employed as an active EL material for the following reasons:

1. DLC films can be deposited with optical bandgaps wide enough to be potentially useful for visible application ($E_{opt} > 2$ eV).
2. Luminescence in DLC is potentially efficient because of the absence of the k-conservation selection rule in an amorphous material.
3. Visible photoluminescence (PL) has been observed in wide optical bandgap DLC films [8-10].

4. EL has been observed in a similar material: amorphous, hydrogenated silicon carbide, a-Si_xC_{1-x}:H [11-13].
5. Unlike ZnS, which is hygroscopic, DLC is relatively insensitive to moisture.

The primary purpose of this thesis is the optimization of electrical and optical properties of DLC films for EL applications. One of the most significant results presented in this thesis is the first observation of electro-luminescence from DLC films.

A literature review of DLC is covered in Chapter 2. A description of the plasma-enhanced chemical vapor deposition (PECVD) system and experimental measurement methods are presented in Chapter 3. Subsequently, the experimental results and a discussion of the results are described in Chapter 4. Finally, in Chapter 5, conclusions are drawn and recommendations for future work are suggested.

Chapter 2. Literature Review of Diamond-like Carbon

Robertson and Angus et al. have extensively reviewed [14,15] the properties of various types of amorphous carbon and hydrogenated amorphous carbon. Tsai & Bogy and Sundgren & Hentzell have reviewed [16,17] DLC films as hard coatings. Meyerson has briefly overviewed [18] the macroscopic film properties of a-C:H. Woollam et al. have provided a bibliography [19] of diamond-like carbon work published from 1956 to early August 1985.

2.1 Nomenclature

There seems to be no standard name for diamond-like carbon; which has also been called amorphous hydrogenated carbon (a-C:H) , polymer-like carbon, and i-carbon which was suggested [20] by Weissmantel et al.(the i comes from ion).

What then are diamond-like carbon films ? Angus has proposed [21] that the hydrocarbon films can be empirically classified by their gram atom number density, ρ_N, and their atomic fraction, X_H, of hydrogen. The gram atom number density, ρ_N, can be expressed by [21]

$$\rho_N = \frac{\rho_M}{\Sigma\ X_i\ A_i} \qquad (2.1)$$

where ρ_M is the mass density, X_i the atom fraction, and A_i the atomic mass of element i. According to Angus, the term "diamond-like" can be used for films having $\rho_N > 0.2$ g atom cm^{-3}, containing significant amounts of hydrogen, and

employing predominant sp^3 over sp^2 bonding. Films with $\rho_N < 0.2$ g atom cm^{-3}, would be called "polymer-like".

2.2 Deposition Methods

Diamond-like carbon (DLC) films have been deposited by several deposition techniques. The most frequently employed techniques for the film production are:

1. Glow-discharge deposition
   a) LF plasma deposition [22]
   b) RF plasma deposition [23]
   c) DC plasma deposition [24]
2. Ion beam deposition
   a) primary ion beam deposition [25]
   b) secondary ion beam deposition [26]

In addition to the above techniques, Hiraki et al. used [27] a reactive rf-sputtering technique in which hydrogen gas was used with a graphite target to obtain DLC films with 80 % sp^3 bonding, a 2.8 eV optical bandgap, and an unpaired electron spin density of 2×10^{17} cm^{-3}. The optical, electrical, and mechanical characteristics of DLC films as a function of different deposition gases and different preparation methods are summarized [16] by Tsai & Bogy.

Matsumoto et al. have reported [28] on the effect of diluent gases, such as hydrogen, argon, and helium in methane. Using a CH_4 and H_2 mixture, they obtained diamond-like clusters containing large amounts of hydrogen, while they obtained graphite with smaller amounts of hydrogen when

using CH_4 and Ar. They also claimed that only graphite was produced using CH_4 by itself, or a CH_4 and He mixture. Their plasma system, however, is somewhat different from others; it employs a 2450 MHz plasma excitation frequency.

Couderc & Catherine have discussed [29,30] the plasma excitation frequency dependence of the physical properties of a-C:H films. Frequencies of 13.56 MHz and 50 kHz were employed to deposit the films. In their report they suggested that the ion bombardment effects of the high frequency (13.56 MHz) and the low frequency (50 kHz) are related to the products (self-bias voltage) x $(\text{pressure})^{-\frac{1}{2}}$ and (current density) x $(\text{pressure})^{-\frac{1}{2}}$, respectively.

2.3 Photoluminescence

Unlike hydrogenated silicon carbide (Si_xC_{1-x}:H), few papers on the photoluminescence of DLC have been reported. Watanabe [8-10] et al., Lin & Feldman [31,32], and Wagner & Lautenschlager [33] have observed white photolumenescence (PL) at room temperature associated with an excitation energy of 2.5-3.4 eV. PL spectra show very weak temperature dependence according to the above papers, but generally the measured PL intensities increase with decreasing temperature. The luminescence peak shifts toward lower energy with increasing deposition temperature, which is correlated with a decrease in optical bandgap, E_{opt}. The optical bandgap increases with the content of hydrogen in the film, as a general tendency.

The role of hydrogen incorporation into the DLC film is controversial. One viewpoint is that hydrogen passivates dangling bonds [35], in a similar manner as the hydrogenation of amorphous silicon. An alternative interpretation [14,34] is that in addition to passivating unpaired spins, the incorporation of hydrogen leads to a microscopic modification of the structure of the DLC film and that this structural modification results in a reduction in the π-defect density. A schematic diagram of the density of states for an amorphous semiconductor which indicates localized defect density is shown in Fig. 2.1.

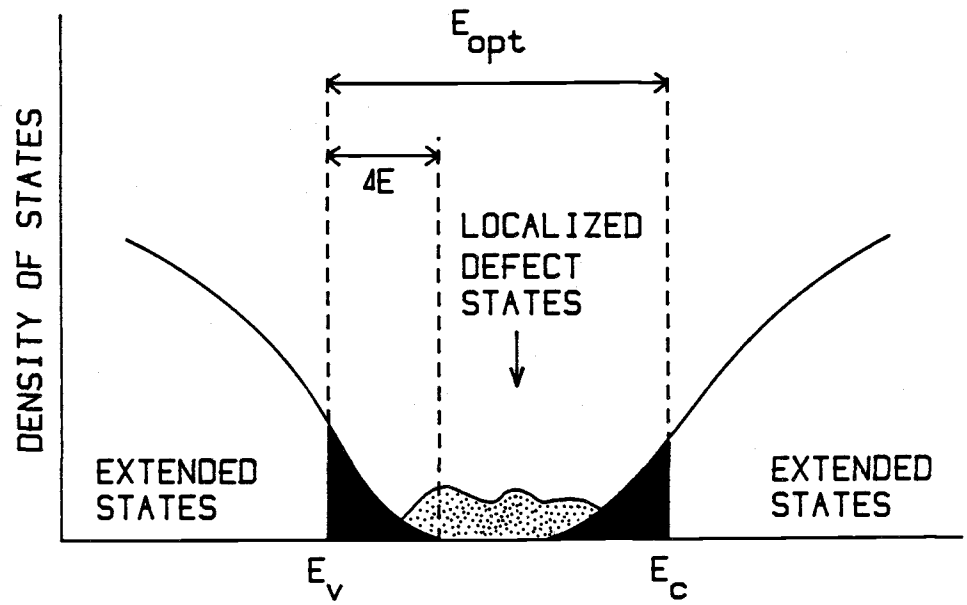

Figure 2.1. A schematic diagram of the density of states for an amorphous semiconductor [43].

2.4 Thermal Annealing

The optical bandgap of a DLC film decreases significantly with increasing anneal temperature. For reduction in the optical bandgap, many workers agree [36-40] that hydrogen evolution from the film causes structural changes in the films and a transition from sp^3 to sp^2 bonding occurs. Dischler et al. found [37] that an as-grown film with 68% sp^3 tetrahedral bonding is reduced to almost 0% sp^3 bonding when annealed at 600 °C (0% of sp^3 bonding means that the film is completely graphitized; therefore, the optical bandgap is zero). Fink et al. also observed [39] a closing of the optical bandgap and a delocalization of the π-electrons between 400 °C and 600 °C. Natarajan et al., however, observed [40] that films prepared by the decomposition of methane or propylene still showed an appreciable optical bandgap even at 800 °C.

Recently, Wild & Koidl found [41] that the hydrogen evolution from a DLC film depends on the bias voltage, U_B, of the plasma in which the film was grown. Films grown at a low bias voltage, $U_B < 400$ V, release both hydrogen and hydrocarbons, whereas films deposited at $U_B > 500$ V lose hydrogen only. They suggest a potential application for these films as a diffusion barriers or as membrane materials with selective permeability.

2.5 Optical Bandgap

As shown in Fig. 2.2, both valence and conduction band edges are composed of π-states in a-C:H. The ratio of π to σ electrons, i.e. the ratio of sp^2 to sp^3 bonding sites, can be evaluated by nuclear magnetic resonance (NMR) measurements [42] or by electron energy loss spectroscopy (EELS) [39].

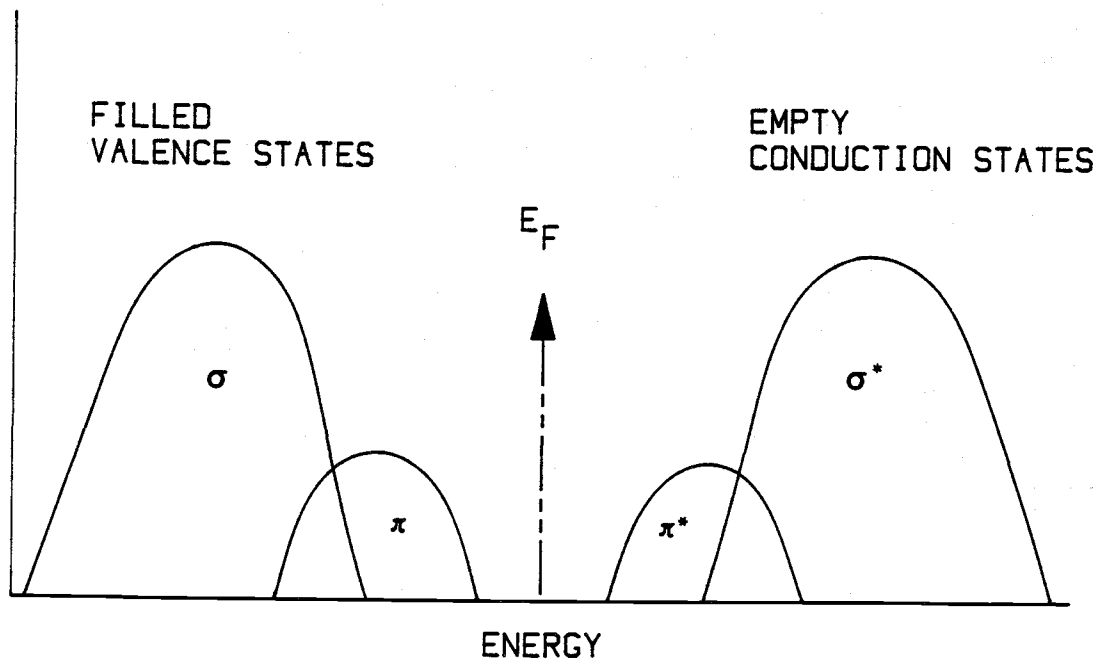

Figure 2.2. A schematic representation of the electronic spectrum of an unsaturated hydrocarbon [14].

One of the most important optical parameters, the optical bandgap, is directly related to the sp^2/sp^3 ratio. Kaplan et al. measured [35] the E_{opt} of various DLC films associated with a hydrogen incorporation in the film. Their results indicate that E_{opt} increases with the amount of the hydrogen incorporated in the film, whereas the hardness.is inversely proportional to that of hydrogen.

Most researchers evaluate the optical bandgap, E_{opt}, from a "Tauc plot" (see section 4.2) of an optical absorption data [43] as given by the following equation

$$\alpha h\nu = B\,(h\nu - E_{opt})^2 \qquad (2.2)$$

where α is the absorption coefficient, h is Plank's constant, ν is the photon energy, and B is a coefficient given by

$$B = 4\pi\sigma_{min}/nc\Delta E$$

where ΔE is the band edge width of the localized tail state (refer Fig. 2.1), c is the speed of light, n is the refractive index, and σ_{min} is the minimum metallic conductivity. In this thesis, above equation is employed to obtain the E_{opt}.

Chapter 3. Experimental Technique

3.1 Plasma-Enhanced Chemical Vapor Deposition System

The physical properties of PECVD grown DLC films depend on process parameters such as power density, pressure, substrate temperature, plasma excitation frequency, flow rate, and electrode spacing. In this section, the behavior of electrons, ions, and free radicals in the plasma are considered in order to elucidate the film growth mechanism.

3.1.1 Description of the PECVD System

A schematic diagram of the plasma-enhanced chemical vapor deposition (PECVD) system is shown in Fig. 3.1. The plasma frequency is either 13.56 MHz or 100 kHz, and the system has a capacitively coupled, parallel plate electrode configuration in which the substrate electrode is grounded. A modified electrode configuration in which the substrate is powered is shown in Fig. 3.2. The system has a built-in programmable microprocessor for automatic control of the process parameters.

The reaction chamber (43 cm in diameter and 10.2 cm in height) and the electrodes are made of aluminum. The electrode areas and the adjustable electrode spacing ranges for the two configurations shown in Figs. 3.1 and 3.2 are listed in Table 3.1.

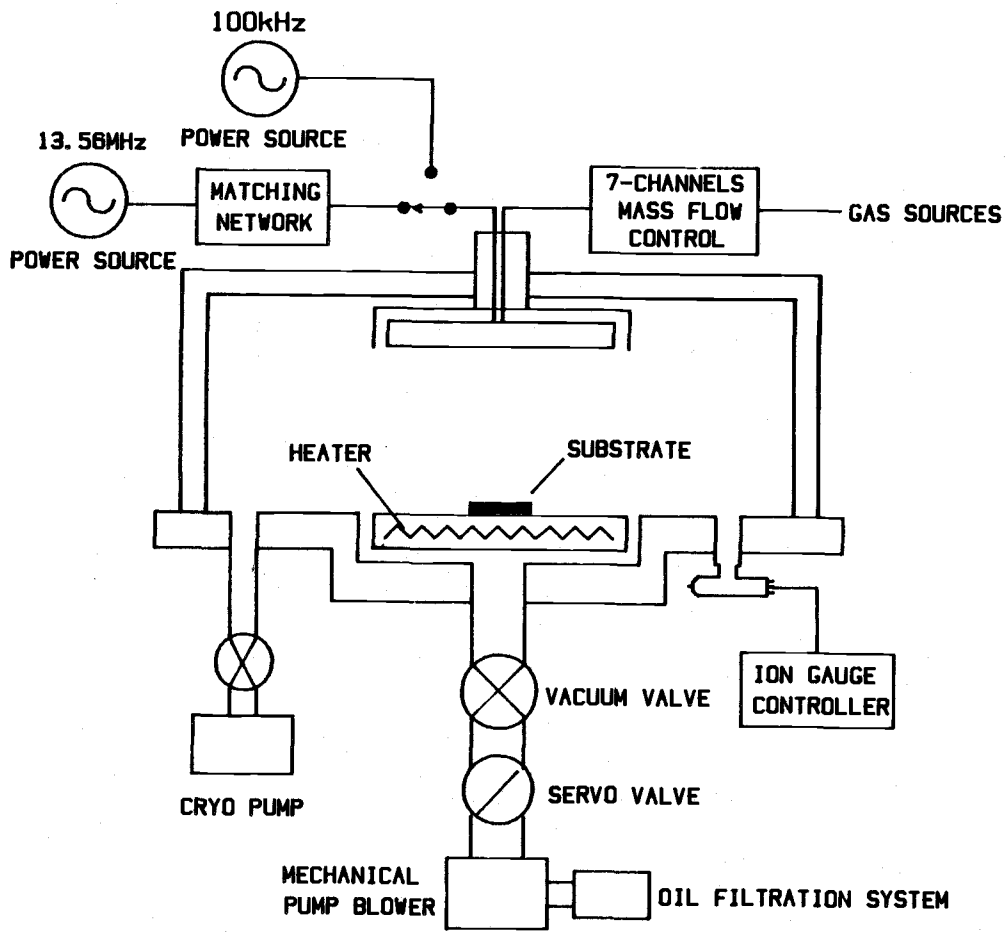

Figure 3.1. A schematic diagram of PECVD system.

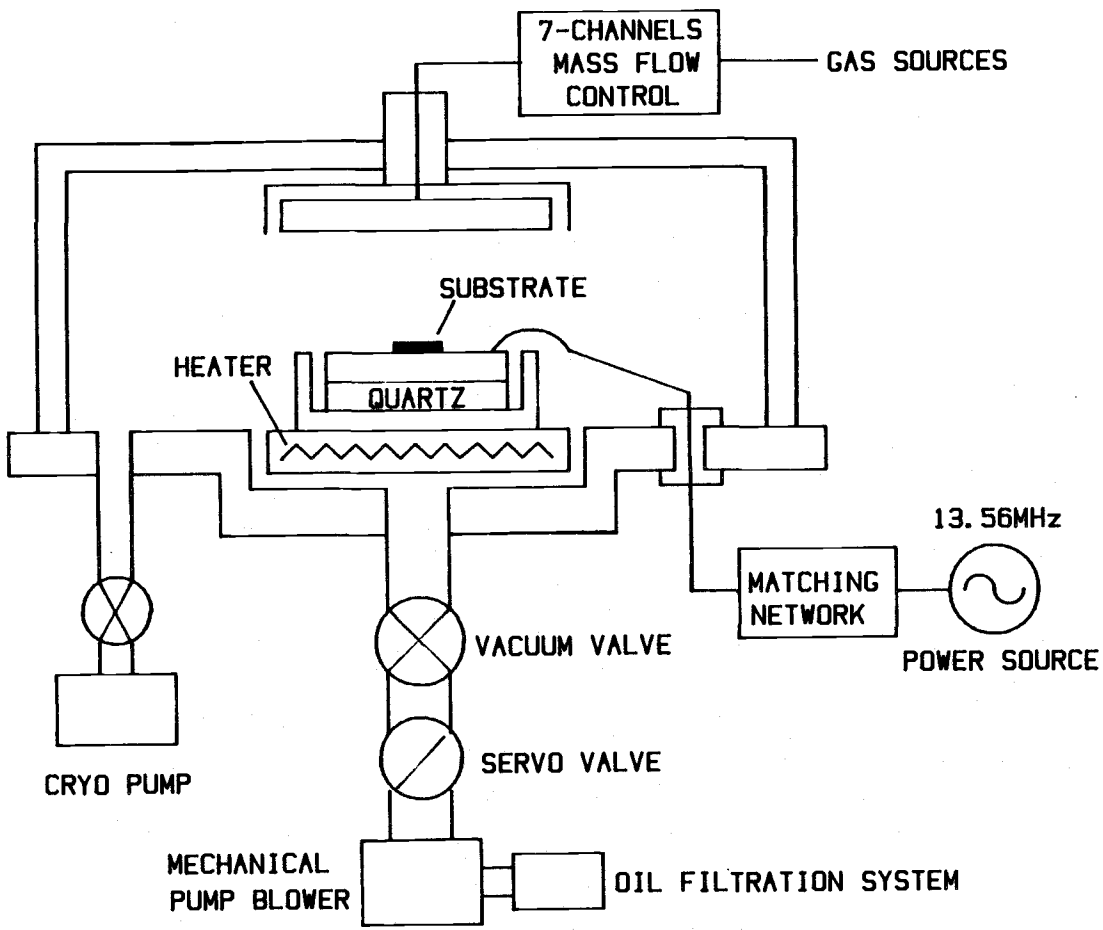

Figure 3.2. A schematic diagram of modified PECVD system.

Table 3.1. Electrode areas and adjustable electrode spacing ranges of the two configurations.

	Area of powered electrode	Area of grounded electrode	Adjustable electrode spacing
Fig. 3.1	670 cm^2	425 cm^2	10 - 50 mm
Fig. 3.2	127 cm^2	670 cm^2	10 - 34 mm

The effective area of the grounded electrode is, however, much larger than the dimensions quoted above because the chamber wall is also grounded.

For the configuration shown in Fig. 3.1, the powered electrode is excited with either a 13.56 MHz rf amplifier (ENI OEM-6) or a variable frequency, 90 kHz-460 kHz, lf amplifier (ENI LPG-6). The rf power is coupled to the top electrode via an impedance matching network (MCS ATN 500M) and the forward and reflected powers are monitored with a power metering unit (MCS ATN 500).

The lf amplifier, which has a built-in impedance matching transformer, can be directly connected to the top electrode by bypassing the rf impedance matching circuit. The reflected and forward powers can be monitored with a power meter attached on the front panel of the LF amplifier.

For the electrode configuration shown in Fig. 3.2, the small substrate electrode (5 inches in diameter) was designed and added to the system. It is powered and isolated from the heated electrode. The substrate sits on the aluminum block which in turn sits on a one-quarter inch thick piece of quartz, which provides both isolation from

the substrate electrode and good thermal conductivity. The actual substrate temperature is somewhat less than the measured temperature, because the thermal conductivity of the quartz is less than that of the aluminum.

The aluminum cylinder in which the substrate electrode and the quartz plate sit acts as a dark space shield to extinguish the fringing field plasma. The rf power at 13.56 MHz is capacitively coupled, passes through a matching network, is fed through a vacuum feedthrough at the base of the reactor chamber, and is connected to the substrate electrode via a coaxial cable. The reflected and forward powers can be monitored with the power meter attached to the front panel of the rf amplifier.

3.2 Glow Discharge Mechanism

A plasma can be defined as a partially ionized gas in which approximately equal numbers of positive and negative charges (typical density: 10^{17}-10^{18} m^{-3}) and an amount of unionized neutral molecules (typically 10^{21} m^{-3}) coexist.

3.2.1 Ion Sheath

The ionized particles (ions and electrons) are accelerated by an externally applied rf field. For each half cycle, the relative travelling distance of the electrons is larger than that of the ions; the mass of the ions is much larger than that of the electrons, and hence the mobility of

the electrons is higher. This results in a higher electron current density ($J_e >> J_i$). This effect is enhanced as the plasma excitation frequency is increased. The center of the glow discharge has a larger concentration of ions than electrons due to the rapid escape of electrons from the discharge. Therefore, this glowing part of the discharge has the highest potential in the plasma system, and this potential is called the plasma potential.

Since $J_e >> J_i$, a negative charge will be quickly built up on the substrate placed on an electrode, and the substrate developes a negative potential with respect to the plasma potential. This charge distribution on a substrate produce a "up-hill" potential for electrons and a "down-hill" potential for ions, as shown in Fig. 3.3. This results in a space charge region between the glow discharge and the substrate. This region is called a sheath in the context of glow discharge plasmas. The sheath region consists of mainly ions. The lack of electrons in the sheath is responsible for much less glow. That is why the sheath is also called a dark space.

An equivalent circuit of a sheath can be represented by a capacitor. Since a sheath forms near each electrode, the plasma system can be regarded as two capacitors connected in series. The potential drop ratio of one sheath over the other sheath depends on the electrode area and can be expressed by [44]

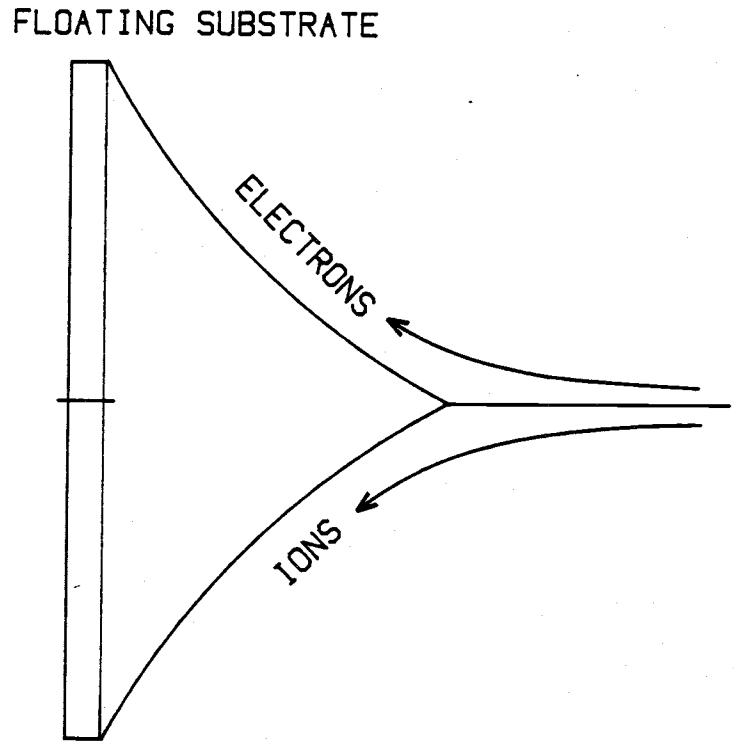

Figure 3.3. Variation of the potential energies of electrons and positive ions in the vicinity of an electrically floating substrate [44].

$$V_1/V_2 = (A_2/A_1)^m \qquad (3.1)$$

where A_1 and A_2 are areas of the powered and grounded electrodes, and V_1 and V_2 are sheath potentials developed near the powered and grounded electrodes, respectively, as shown in Fig. 3.4. The exponent m has a value between 1-4 depending on the geometry of the asymmetric system. The above equation implies that the sheath potential increases

with decreasing area of the electrodes. The larger potential drop, which is slightly less than the peak value of the applied voltage, drops across the sheath formed near the smaller electrode.

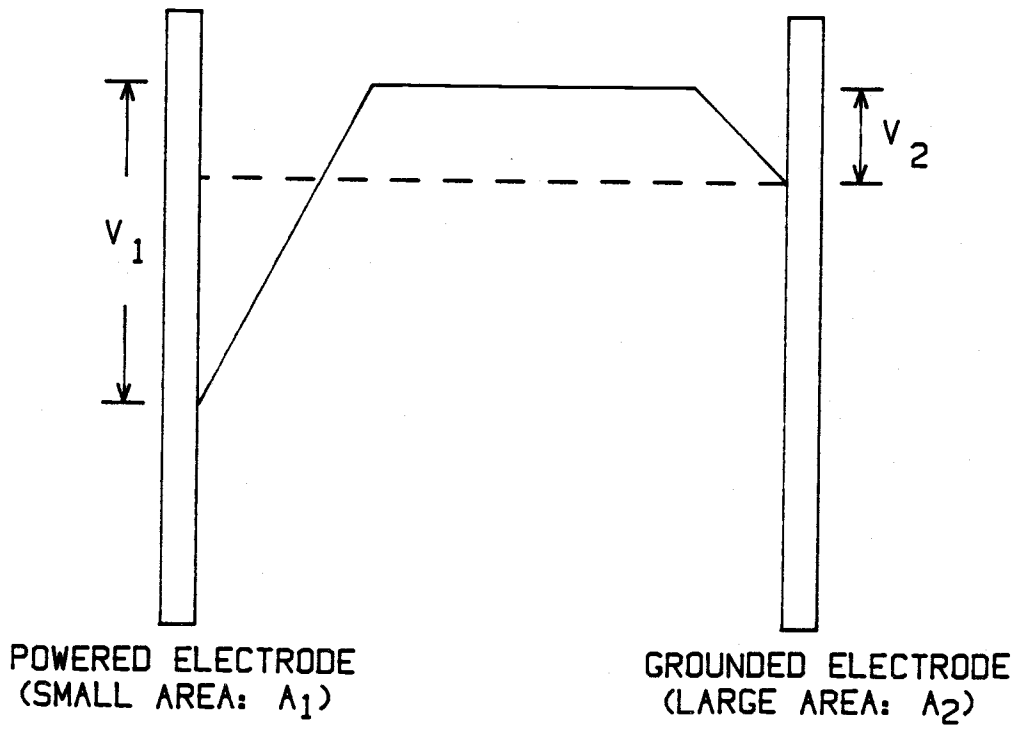

Figure 3.4. Voltage distribution in a rf glow discharge system (with blocking capacitor) [44].

3.3 Deposition of Diamond-like Carbon Films

DLC films are deposited using three different system configurations as described in section 3.1.1. These configurations are:

(a) Unmodified electrode configuration (Fig. 3.1: substrate electrode is grounded) with a plasma excitation frequency of 13.56 MHz.

(b) Same electrode configuration of (a), but with a plasma excitation frequency of 100 kHz.

(c) Modified electrode configuration (Fig. 3.2: substrate electrode is powered) with a plasma excitation frequency of 13.56 MHz.

Hereafter, DLC films from configuration (a) will be called HF (high frequency) DLC films, from configuration (b) LF (low frequency) DLC films, and from configuration (c) PWRD (powered substrate) DLC films, respectively. These modes of deposition are now discussed.

3.3.1. HF DLC films

The mechanical pump and the filtration system are warmed up for 30 minutes before operation. The substrate (Si-wafer or quartz) is cleaned with acetone and methanol in an ultrasonic bath, dried by N_2 gas after rinsing with deionized (DI) water, and placed on the bottom electrode which is parallel to the top electrode. The deposition parameters, such as power, substrate temperature, processing

time, deposition pressure, and flow rate are preset using a built-in microprocessor control. While the bottom electrode is heating up to the preset deposition temperature, the reactor is pumped down for about 5 minutes with a mechanical pump. When the pressure reading is 2-3 mT, the Cryopump is operated for 15 minutes to reduce the chamber pressure to about 10^{-5} Torr. This minimizes the contamination prior to deposition.

The chamber pressure is monitored with either a capacitance manometer (MKS BARATON TYPE 227A) in the range 2 - 999 mT, or an ionization gauge control (MKS TYPE 290) for the range from 10^{-3} - 10^{-7} Torr. The capacitance manometer controls a throttle valve (VACUUM CENTRAL MDV-018) to keep a constant pressure during the deposition. When the operation of the Cryopump is finished, the reactor is purged by the source gas (10 % CH_4 diluted in helium) for 5 minutes. When the deposition temperature has stabilized, the source gas is introduced into the reactor with a flow rate from 10 - 30 SCCM (Standard Cubic Centimeters per Minute). The flow rate is controlled by a mass flow controller (MKS type 2259A). When the deposition pressure has stabilized at the preset value, the preset power (6 W - 150 W) is applied to the reactor, and the glow discharge is observed through a window installed on the reactor. The deposition process lasts for a preset process time (30 minutes - 3 hours). DLC films are deposited at different powers, substrate temperatures, pressures, and electrode spacings. This deposition

process can be accomplished by either manual or automatic operation.

3.3.2. LF DLC films

The deposition procedure for LF DLC films is the same as for HF DLC films except the output terminal of the variable frequency amplifier (90 kHz - 460 kHz) is directly connected to the top electrode, bypassing the impedance matching circuit ,and the electrode spacing is re-adjusted to 50 mm.

3.3.3. PWRD DLC films

The modified substrate electrode is placed on the bottom heatable electrode, and is reconnected to the output of the rf amplifier through the matching network. Other than that, deposition procedure is identical to the deposition process of HF DLC films.

3.4 Measurement of Physical Properties of DLC Films

3.4.1 Optical Bandgap

The optical bandgap, E_{opt} is determined from optical absorption measurements over a photon energy range of 1.5-6.5 eV (190 nm-820 nm in wavelength) using a Hewlett-Packard 8451 Diode Array Spectrophotometer. For the optical absorption measurements, DLC films are deposited on a piece

of quartz substrate (1" x 1" in size) which is cut half from a quartz slide (1" x 2" in size), and the other half piece is used as a reference to eliminate the background effects.The background effects are cancelled in the computer. The reflectance at the film surface, however, is not corrected in the measurement.

The raw data from the spectrophotometer is an absorbance vs. wavelength plot, where the definition for the absorbance,A, is

$$A = -\log T \qquad (3.2)$$

$$T = I/I_o \qquad (3.3)$$

where T is the transmission rate, I_o the incident photon energy, and I the transmitted photon energy. Additionally,

$$I = I_o \exp(-\alpha\ d) \qquad (3.4)$$

where α is the absorption coefficient, and d the film thickness. From equations (3.2) and (3.4),

$$A/d = \alpha\,. \qquad (3.5)$$

The film thickness,d, is measured with a Dektak mechanical profilometer. Therefore, the Y-axis (absorbance) of the raw data can be rescaled as absorption coefficient, and the X-axis (wavelength) can also be rescaled as photon energy (eV) by the use of a simple HP basic program. Thus, the absorption coefficient, α, vs. photon energy, $h\nu$, plot is obtained. Finally, the absorption coefficient axis is rescaled and the $(\alpha h\nu)^{\frac{1}{2}}$ vs. $h\nu$ plot is obtained. From this plot, E_{opt} can be determined by extrapolating the graph to

the X-axis. The intercept with the X-axis is defined as E_{opt} (refer to section 2.5).

3.4.2. Photoluminescence Spectrum

DLC films are deposited on a Si-wafer for photoluminescence (PL) measurements, which were accomplished using a 9-15 mW Ar laser at a wavelength of either 4880 Å (2.54 eV) or 5140 Å (2.41 eV). Most of the PL spectra were measured at room temperature. However, a few samples were measured at 13 K to determine the temperature dependence of PL peak. A S1 photomultiplier tube (PMT) was used in these measurements.

3.4.3 Current-Voltage Characteristics

Current-voltage (I-V) measurements were made using an Hewlett-Packard 4061A Semiconductor Component Test System on metal-insulator-simiconductor (MIS) structures, with the DLC film acting as an insulator. Aluminum was evaporated on the rear side of a p-type Si-wafer for ohmic contact and evaporated on the DLC films through a metal mask for a probe contact.

3.4.4 Film Thickness and Refractive Index

The thickness and refractive index of the DLC films were determined using a Gaertner L117 ellipsometer at a

fixed wavelength of 6328 Å. The films, as measured, had been deposited on a silicon wafer.

3.4.5 Dielectric Constant.

To determine the dielectric constant, capacitance measurements were made on a metal-insulator-metal (MIM) structure, with the DLC film as an insulator, using an Hewlett-Packard 4280A 1 MHz C meter/C-V Plotter. For contact, aluminum dots (dot area: 4×10^{-3} cm^2) were evaporated on the DLC film through a metal mask.

The dielectric constant of DLC can be extracted from the measured capacitance, C, using

$$\epsilon_D = (C\ d)/(\epsilon_o\ A) \qquad (3.6)$$

where ϵ_o= permittivity of free space
A= Aluminum dot area
d= film thickness

The thickness of the DLC film was measured using a Dektak mechanical profilometer.

3.5 Fabrication of the Electroluminescent Device

The structure of the DLC EL device is shown in Fig. 3.5. The glass slide substrates coated with indium tin oxide (ITO) and silicon oxynitride (the bottom insulator) were supplied by Planar Systems of Beaverton, Oregon.

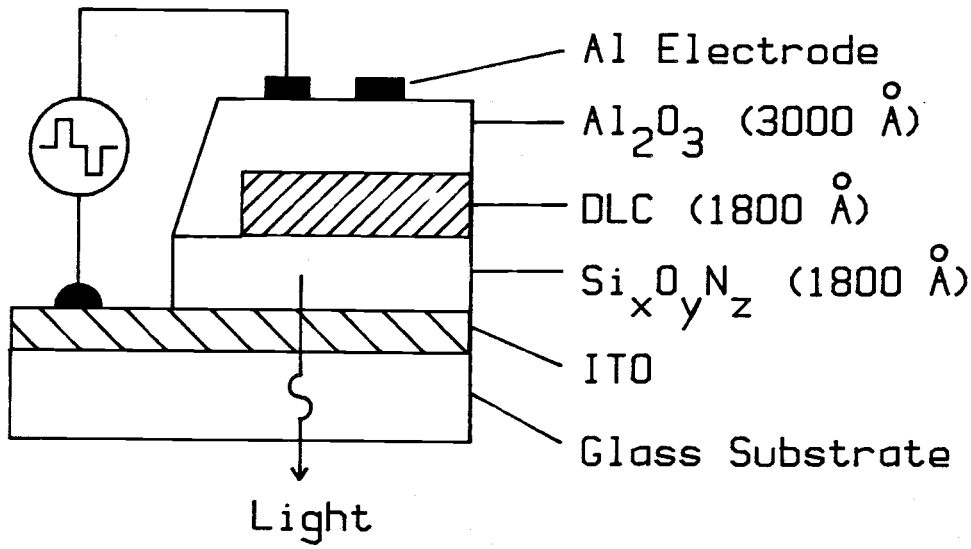

Figure 3.5. Structure of the DLC ACTFEL device.

The fabrication proceeded as follows: one of the three types of DLC films (defined in section 3.3) was deposited on the bottom insulator as an active layer. The deposition parameters for those three types of DLC films are summarized in Table 3.2.

Table 3.2. Summary of the deposition parameters of DLC films developed for EL applications.

	HF DLC film	LF DLC film	PWRD DLC film
Temperature	50 °C	100 °C	250 °C
Power Density	87 mW/cm^2	18 mW/cm^2	175 mW/cm^2
Pressure	800 mT	950 mT	800 mT
Frequency	13.56 MHz	100 kHz	13.56 MHz
Electrode Spacing	16.7 mm	50 mm	34 mm

Subsequently, an aluminum oxide (Al_2O_3) film (the top insulator) was deposited on the active layer. The Al_2O_3 film (2000-2700 Å in thickness) was deposited at room temperature in a Veeco 3-inch Microetch System by secondary ion beam sputtering, using an Al target and N_2O as a reactive sputtering gas (The advantage of Al_2O_3 is low deposition temperature, which ensures compatibility with low temperature deposited DLC films, and its high dielectric constant (ϵ = 9-11 compared to ϵ = 7 for Si_3N_4), which results in less voltage drop across the insulator for equal film thickness).

The process parameters of Al_2O_3 films for EL device applications are shown in Table 3.3.

Table 3.3. Process parameters of Al_2O_3 films.

Acceleration Voltage	: 800 V
Target current	: 70 mA
Pressure	: 1.5×10^{-4} Torr
Target/substrate distance	: 6 cm

Finally, aluminum (the second electrode) is evaporated on the top insulator through a metal mask.

3.5.1 Electroluminescence Spectrum Measurements

EL devices are tested by measuring the emission spectrum induced by the application of an ac voltage between the ITO and the aluminum electrode. A schematic diagram of the EL spectrum measurement system is shown in Fig. 3.6.

A 10 kHz pulse wave with a duty cycle of approximately 20% was used, and the amplitude was progressively increased until luminescence was observed. Typical voltage amplitudes used were 200-300 V.

3.5.2. Brightness-Voltage, Efficiency-Voltage, and Brightness-Frequency Measurements

Brightness-voltage (B-V), efficiency-voltage (E-V), and brightness-frequency (B-F) measurements on EL devices were performed at Planar Systems. A block diagram of the measuring system is shown in Fig. 3.7, in which the two parallel leads, oppositely coupled, pass through the loop of the current probe. The displacement current which flows through the EL device with conduction current can be cancelled by this circuit configuration by adjusting the resistor-capacitor balance network (R.C. BAL). By doing so, the consumed power in the EL device was measured by multplying the applied voltage and the conduction current.

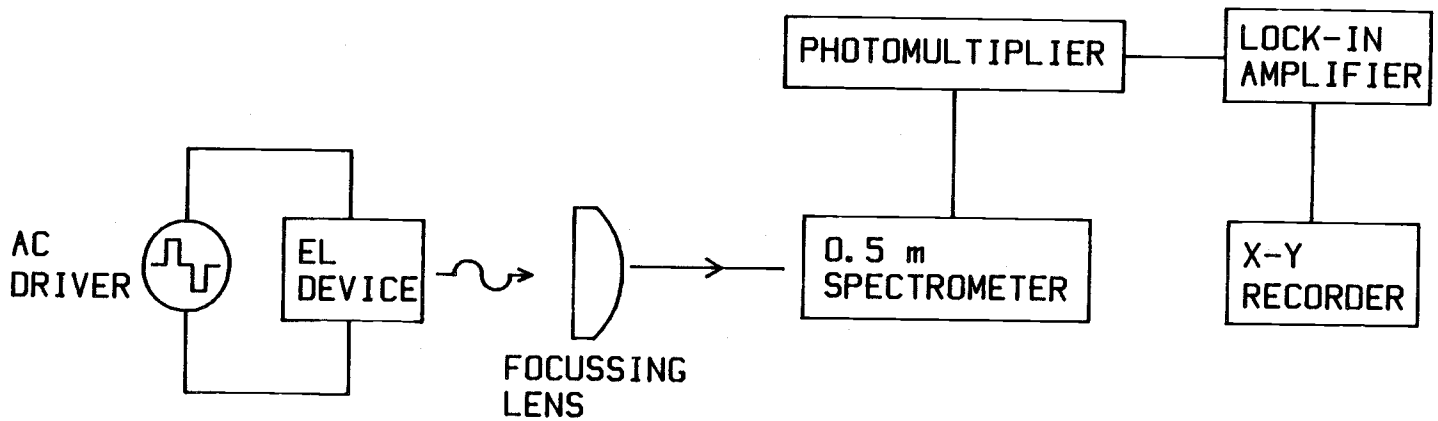

Figure 3.6. A schematic diagram of the EL spectrum measurement system.

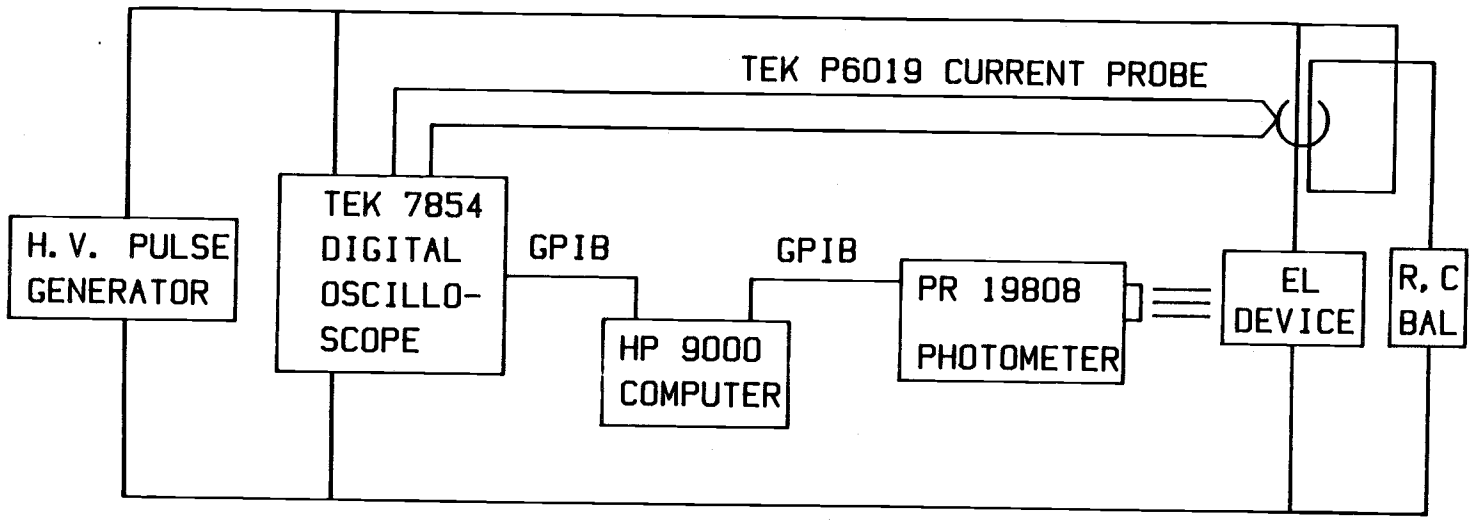

Figure 3.7. A block diagram of measuring system for the B-V, E-V, and B-F characteristics.

The efficiency is defined by

$$\eta = \frac{\text{optical output}}{\text{electrical input power}}$$

The optical output, i.e. the brightness, was measured by a PR 1980B photometer. The B-V and E-V characteristics were measured simultaneously using an Hewlett-Packard 9000 computer control. The B-F characteristics were measured in the range of frequency from 60 Hz-6 kHz.

Chapter 4. Experimental Results and Discussion

4.1 Deposition of DLC Films

4.1.1 DLC Films by High Frequency Plasma Excitation

As shown in Table 4.1, no observable deposition is obtained above a substrate temperature of 200 °C with an electrode spacing of 22.5 mm. Warner et al. have reported [45] a similar observation. This decrease in the growth rate of DLC films at elevated temperatures is apparently due to

Table 4.1. Optical bandgap and film thickness of DLC films deposited at various temperatures and powers. The electrode spacing was 22.5 mm and the deposition time was 30 minutes.

Temperature (°C)	Power (W)	Optical bandgap (eV)	Film thickness (Å)
50	10	3.0±0.5	900
	27	2.5	1500
	67	2.5	3000
100	10	2.7±0.5	720
	27	2.7	1400
	67	2.6±0.1	2400
150	10	2.4±0.2	360
	27	2.9±0.1	1200
	67	2.8±0.1	2200
200	10	x	0
	27	2.5±0.3	500
	67	2.7	1300
300	27	x	0
	67	x	0
	100	x	0
	150	x	0

the propensity of by-products,such as hydrogen, to etch the growing film. As the temperature is increased, the hydrogen becomes more active. Yasuda and Hirotsu have identified [46] plasma activated hydrogen as a DLC etchant, and Hoffman et al. have employed [47] a mixture of argon and hydrogen to intentionally etch DLC films.

When the electrode spacing is reduced to 14.5 mm, an appreciable deposition rate is observed up to a substrate temperature of 300 °C, as shown in Table 4.2. It is not

Table 4.2. Optical bandgap and film thickness of DLC films deposited at various temperatures and powers. The electrode spacing was 14.5 mm and the deposition time was 30 minutes.

Temperature (°C)	Power (W)	Optical bandgap (eV)	Film Thickness (Å)
50	10	3.0±0.4	800
	27	2.9±0.1	1500
	67	2.4	4500
100	10	3.0±0.5	600
	27	2.7±0.2	1900
	67	2.6	3000
150	10	3.0±0.5	500
	27	2.6	1500
	67	2.3	3000
200	10	2.6±0.2	360
	27	2.8±0.1	1300
	67	2.4	2300
250	10	x	0
	27	2.9±0.1	800
	67	2.4	2800
300	10	x	0
	27	2.2±0.1	400
	67	2.4	1000

clear why the DLC growth rate increases with a decrease in the electrode spacing. One possibility is that the reduced electrode separation results in more efficient plasma generation and a concomitant increase in the impingement flux of free radicals. Alternatively, the substrate sheath potential will increase as the electrode spacing decrease as a consequence of the reduced effective area of the ground electrode (see equation 3.1) which could conceivably increase the deposition rate because of the increase in the ion flux. Further work is necessary to inequivocally resolve this issue.

The I-V characteristic of a HF DLC film is shown in Fig. 4.1. An optimized HF DLC film displays a breakdown field (defined as the field at which the current equals 1 μA) of 3.1 MV/cm, and a resistivity of 2 x 10^{13} ohm-cm at 1 MV/cm.

4.1.2 DLC Films by Low Frequency Plasma Excitation

As show in Table 4.3, LF DLC films are obtained at a deposition temperature of 300 °C, even with an electrode spacing of 25 mm.

The LF DLC films deposited exibited scratch free surfaces. They resisted razor blade scratches; in contrast, the HF DLC films could be scratched using a fingernail.

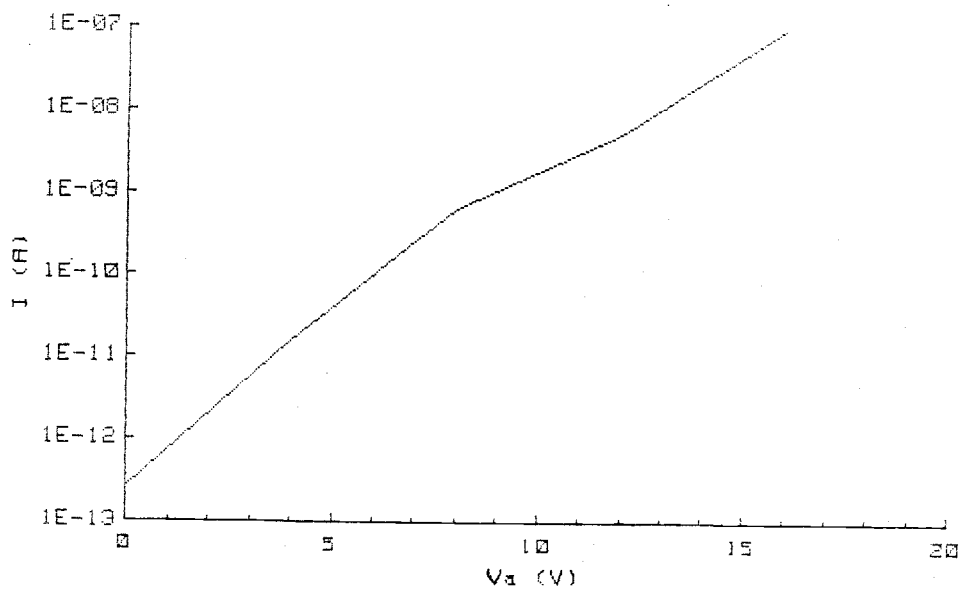

Figure 4.1. I-V characteristic of a HF DLC film.

Table 4.3. DLC films deposited at various temperatures. The power is fixed at 30 W. The electrode spacing is 25 mm and the deposition time is 30 minutes. The plasma excitation frequency is 100 kHz.

Temperature(°C)	Film thickness(Å)	Refractive Index
100	1054	2.11
150	930	2.28
200	839	2.24
250	716	2.26
300	594	2.24

In the case of LF DLC films, the ions can move in phase with the slowly changing polarity, and hence can reach the

substrate. This results in ion bombardment of the substrate and ejection of hydrogen from the film surface during growth, producing a film with less hydrogen and with stronger chemical bonding. Consequently, the LF DLC films are harder.

Variation of the refractive index and field strength of LF DLC films deposited at different temperatures are shown in Fig. 4.2. The refractive index increased with increasing temperature, whereas the field strength decreased.

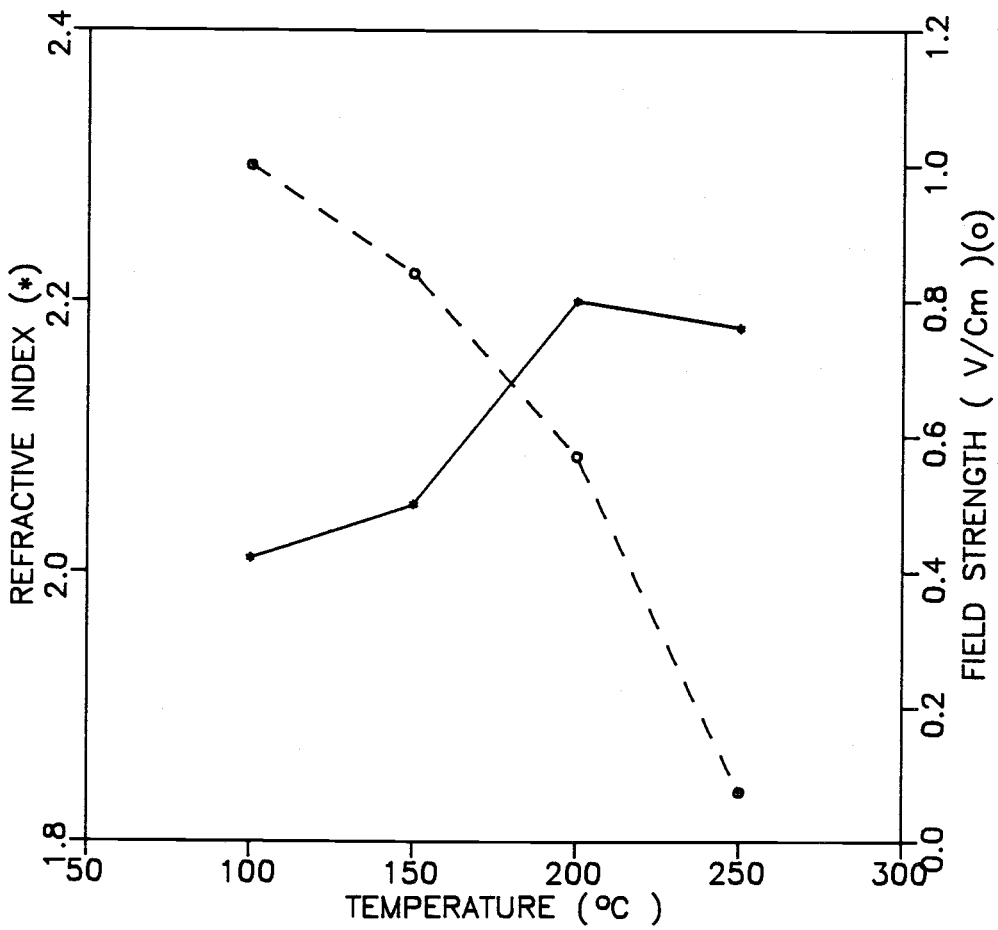

Figure 4.2. Variation of the refractive index and field strength of LF DLC films deposited at different temperatures.

The breakdown field and resistivity of an optimized LF DLC film deposited at 100 °C were 3.2 MV/cm and 4 x 10^{13} ohm-cm, respectively.

4.1.3 DLC Films from the Modified Electrode Structure

The electrode was modified for the purpose of obtaining a better compromise between the mechanical hardness and optical bandgap of the film. The refractive index and film thickness of PWRD DLC films prepared at various pressures are shown in Table 4.4. Films deposited at low pressure were harder and had a smaller optical bandgap than DLC films deposited at higher pressures. This makes sense since the pressure controls the mean free path of gas phase collisions in the plasma; at high pressures depositing species undergo

Table 4.4. Film thickness and refractive index of PWRD DLC films deposited at various pressures. The following deposition parameters are set: power, 40 W; Temperature , 250 °C; electrode spacing, 34 mm; process time, 30 minutes.

Pressure(mT)	Refractive Index	Film Thickness(Å)
250	1.91	633
500	1.65	1182
600	1.60	1175
700	1.57	1222
800	1.56	1286
900	1.56	1275

many inelastic collisions prior to reaching the substrate and thus impact the substrate with reduced kinetic energy.

The films show the highest index of refraction and the lowest deposition rate at a pressure of 250 mT. With this electrode system the operating pressure range was 250-999 mT.

The breakdown field and resistivity of an optimized PWRD DLC film were 1.2 MV/cm and 4 x 10^{11} ohm-cm, respectively.

4.2 Optical Bandgap

One of the most significant physical parameters to optimize in DLC films for EL applications is the optical bandgap, E_{opt}. E_{opt} should be at least about 2 eV or above for visible applications, because the visible wavelength range is 400 nm-700 nm (1.8-3.1 eV in energy).

A Tauc plot, $(\alpha h\nu)^{\frac{1}{2}}$ vs. $h\nu$, for a PWRD DLC film is shown in Fig. 4.3. E_{opt} is determined [43] by fitting the absorption edge spectrum to the expression

$$\alpha h\nu = B\ (h\nu - E_{opt})^2. \qquad (4.1)$$

Note that the expression requires the density of states to be parabolic at each band edge. From Fig. 4.3, E_{opt} could be estimated as either 2.2 eV or 2.9 eV since there are two linear portions of the curve near threshold.

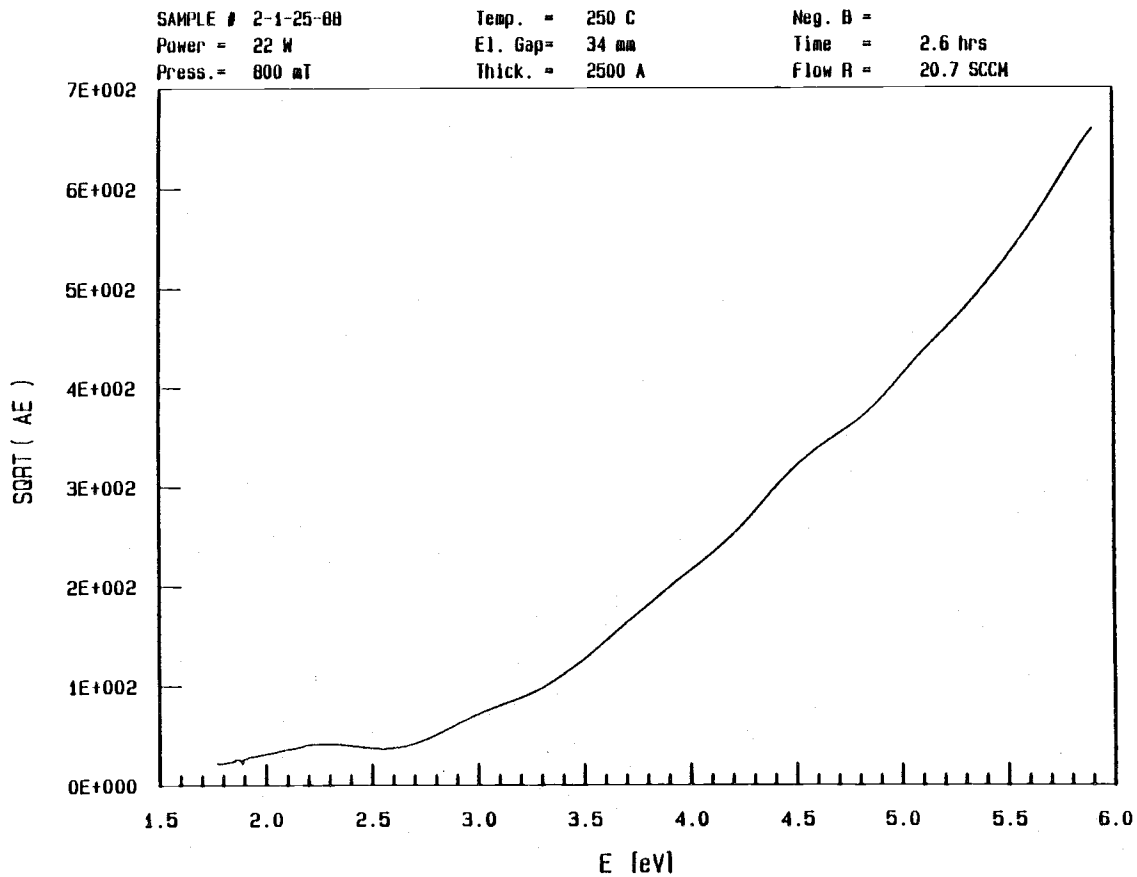

Figure 4.3. Tauc plot for a PWRD DLC film.

The estimated values of E_{opt} for HF DLC films are summarized in Table 4.1 and Table 4.2. It is evident from these Tables that E_{opt} decreases slightly with increasing rf power and substrate temperature. Additionally, as shown in Table 4.5, E_{opt} is relatively independent of the chamber pressure. These trends are in contrast to those observed by other workers [40,48-49]; increasing the rf power or substrate temperature and decreasing the chamber pressure typically results in a significantly reduced E_{opt}. One of the reasons for these results is the minimization of atomic bombardment damage to the growing film, which was achieved by using helium as a diluent gas; the small mass of helium, and hence its kinetic energy, results in less atomic bombardment damage than when standard diluent gases, such as argon, are used. Atomic bombardment damage is also minimized in the unmodified PECVD system, because the substrate electrode is large and at ground potential, which results in

Table 4.5. Optical bandgap and film thickness of HF DLC films deposited at various pressures. The electrode spacing was 22.7 mm, the deposition time was 30 minutes, the substrate temperature was 150 °C, and the excitation power was 27 W.

Pressure (mT)	Optical bandgap (eV)	Film Thickness (Å)
300	2.9± 0.1	1200
400	3.0± 0.3	1000
500	3.1± 0.3	1000
600	3.0± 0.3	1000
700	3.0± 0.3	1000

a small sheath potential and hence, a small kinetic energy of ions impacting the growing film.

The optical gap reduction associated with thermal annealing is shown in Table 4.6. As can be seen from the Table, there is not a large reduction in E_{opt} upon post-annealing; the limited extent of the reduction in E_{opt} may be acceptable for ACTFEL applications. Additionally, this reduction in E_{opt} is associated with the loss of hydrogen from the DLC film. This loss may be minimized during the subsequent ACTFEL insulator deposition since the DLC film is encapsulated by the growing insulator during the deposition. Further work is required to fully assess the viability of employing low temperature deposited DLC films for ACTFEL applications.

Table 4.6. Post-annealing effects of the HF DLC films. These data were taken after thermal annealing in a N_2 atmosphere: temperature, 250 °C; pressure, 500 mT; annealing time, 20 minutes. Deposition parameters were: pressure, 800 mT; process time, 30 min; electrode spacing, 14.5 mm; flow rate, 20.7 SCCM of CH_4; electrode area, 425 cm^2.

sample #	Substrate temperature	Power	E_{opt} of as-deposited films	E_{opt} after thermal annealing	ΔE_{opt}
1-4-24	50 °C	27W	2.8 eV	2.3 eV	0.5 eV
4-4-24	100 °C	67W	2.4 eV	2.2 eV	0.2 eV
2-4-26	150 °C	27W	2.6 eV	2.3 eV	0.3 eV
5-4-02	200 °C	27W	2.8 eV	2.5 eV	0.3 eV
8-4-26	250 °C	27W	2.9 eV	2.5 eV	0.4 eV
1-4-27	200 °C	67W	2.6 eV	2.2 eV	0.4 eV

4.3 Photoluminescence

The room temperature photoluminescence (PL) spectrum of a PWRD DLC film grown at 250 °C, an excitation power of 22 W, a pressure of 800 mT, and an electrode spacing of 34 mm is shown in Fig. 4.4. A broad emission band, centered at approximately 2.3 eV is observed and a secondary shoulder is evident at about 1.95 eV while E_{opt} for this film was either 2.2 eV or 2.9 eV (refer to Fig. 4.3). The two PL peaks appear to be associated with the two absorption edges, although the PL peaks are shifted to lower energies. Similar PL spectra have been reported [8-10,32] by other workers. The PL mechanism has been attributed [8] to radiative transitions between conduction band and valence band tail states.

The PL spectra of a PWRD DLC film, associated with optical pumping energies 2.54 eV and 2.41 eV, are shown in Fig. 4.5. The PL spectrum induced by the lower energy, 2.41 eV, shows three periodic peaks. A similar observation has been reported [31] by Lin and Feldman. These periodic oscillations have been attributed to localized electron-hole pairs created by the lower pumping energy. The period of these oscillations was approximately 0.18 eV, which corresponds to C-H wagging mode energy. This effect disappears when the higher pumping energy is used, because the electron-hole pairs are created at extended states.

PL spectra of HF DLC films deposited at various deposition powers are shown in Fig 4.6. The DLC film

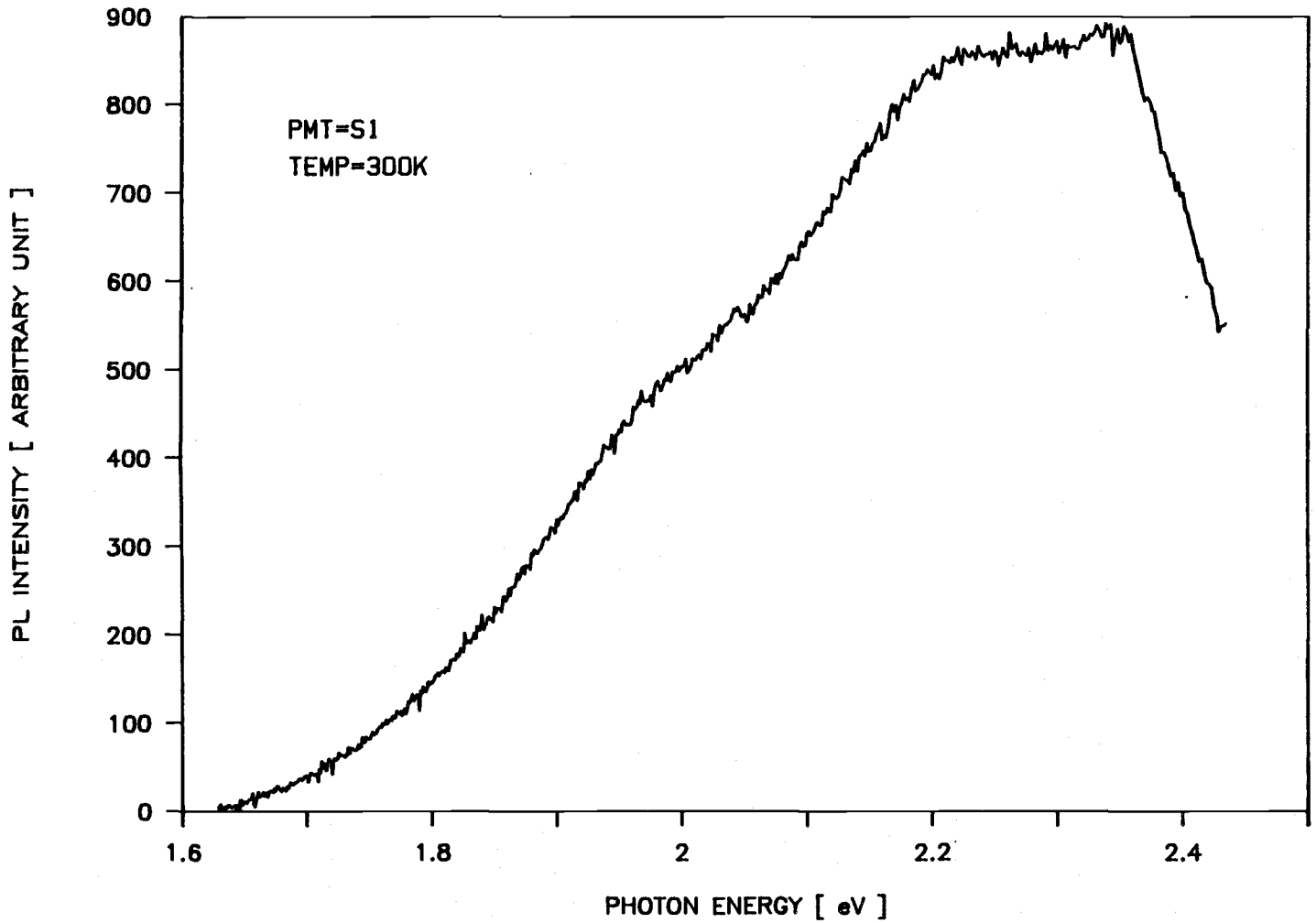

Figure 4.4. The room temperature PL spectrum of a PWRD DLC film.

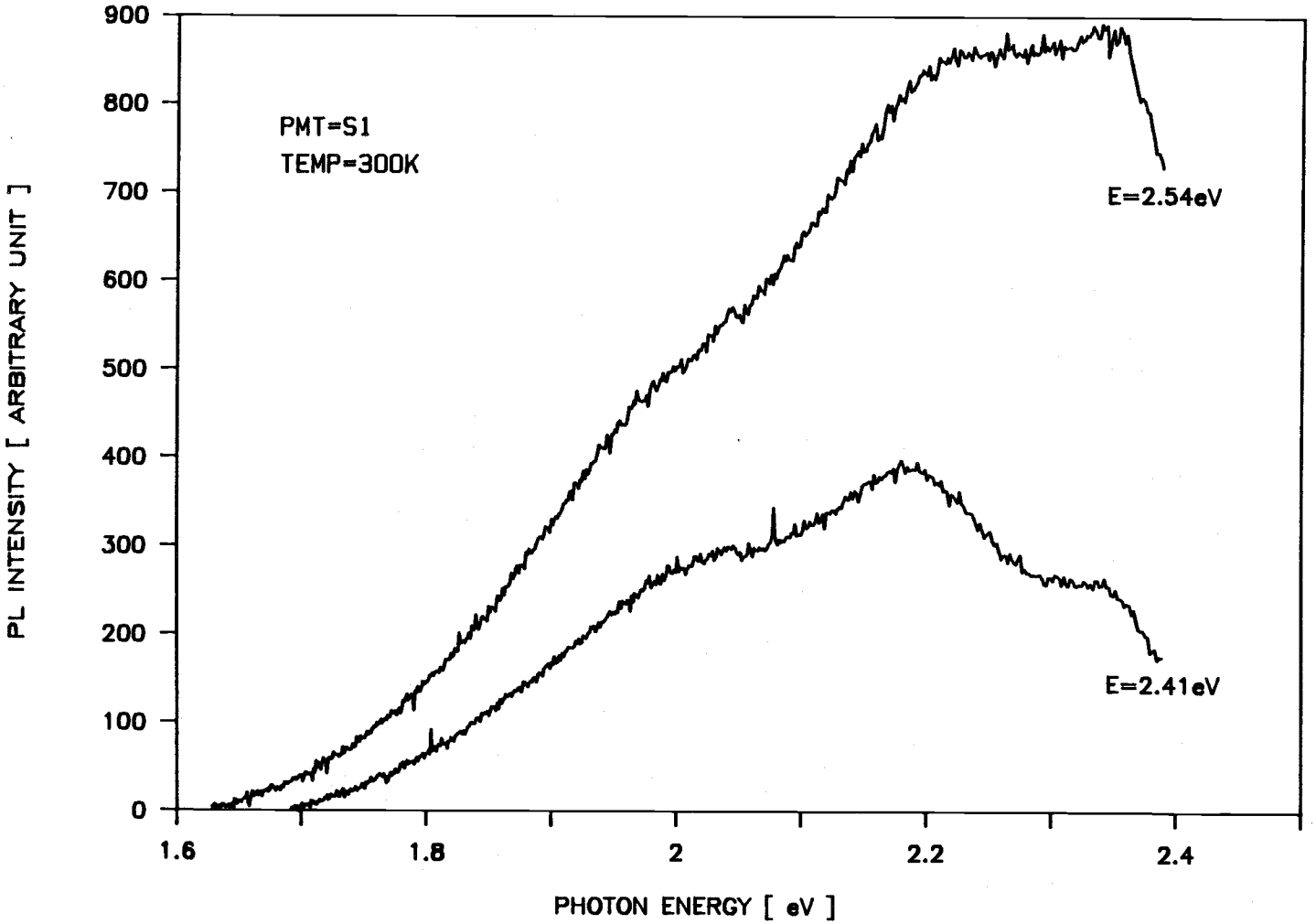

Figure 4.5. PL spectra of a PWRD DLC film associated with optical pumping energies 2.54 eV and 2.41 eV.

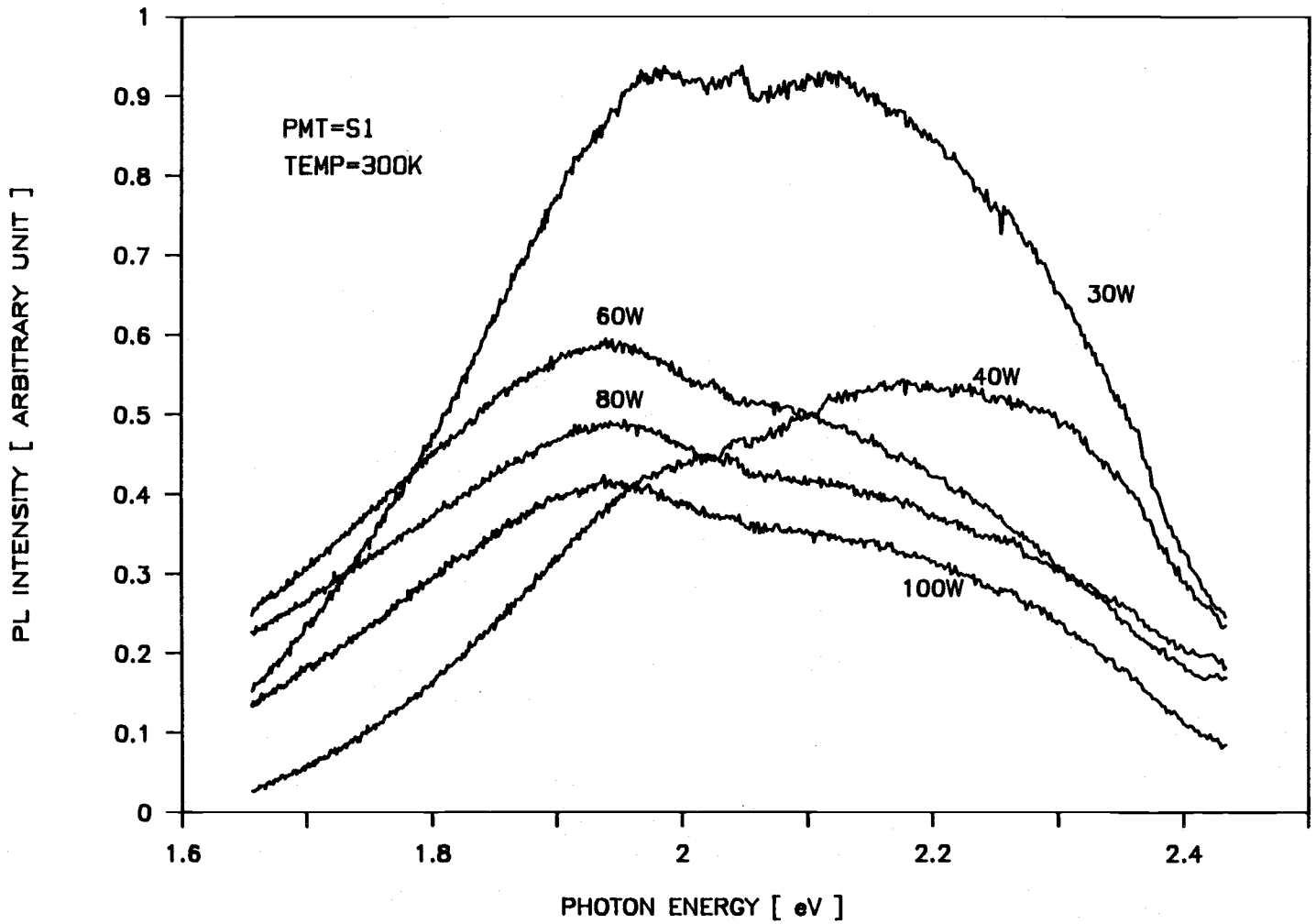

Figure 4.6. PL spectra of HF DLC films deposited at various deposition powers.

deposited at 30 W show two broad emission bands, centered at 1.95 and 2.1 eV, while the 40 W DLC film has a main PL peak at 2.2 eV. The main PL peak of the 60 W DLC film shifts to a lower energy, 1.93 eV. Above 60 W of deposition power, no additional PL peak shifts are observed. The relative PL intensity, however, decreases with increasing deposition power.

The PL peak shifts are attributed to modifications of the defect density located in the forbidden bandgap; high deposition power causes ion bombardment on the growing films, and hence the defect density located in the band tail states is increased.

PL spectra of HF DLC films measured at 13 K and 300 K are shown in Fig. 4.7. The PL spectrum measured at room temperature shows a main peak at 1.95 eV and a secondary peak at 2.15 eV, while the main peak of the PL spectrum measured at 13 K is at 2.2 eV. The main PL peak at 300 K is nearly identical to the secondary PL peak at 13 K.

The shift of the main PL peak from 1.95 eV to 2.2 eV by decreasing the measuring temperature from 300 K to 13 K differs from other results [31] in which the PL spectra are unchanged by temperature reduction, even when the sample temperature was reduced to 2 K. The growth in the PL intensity and the shift in the main PL peak is attributed to a reduction in the probability of nonradiative recombination in the band tail states at low temperature.

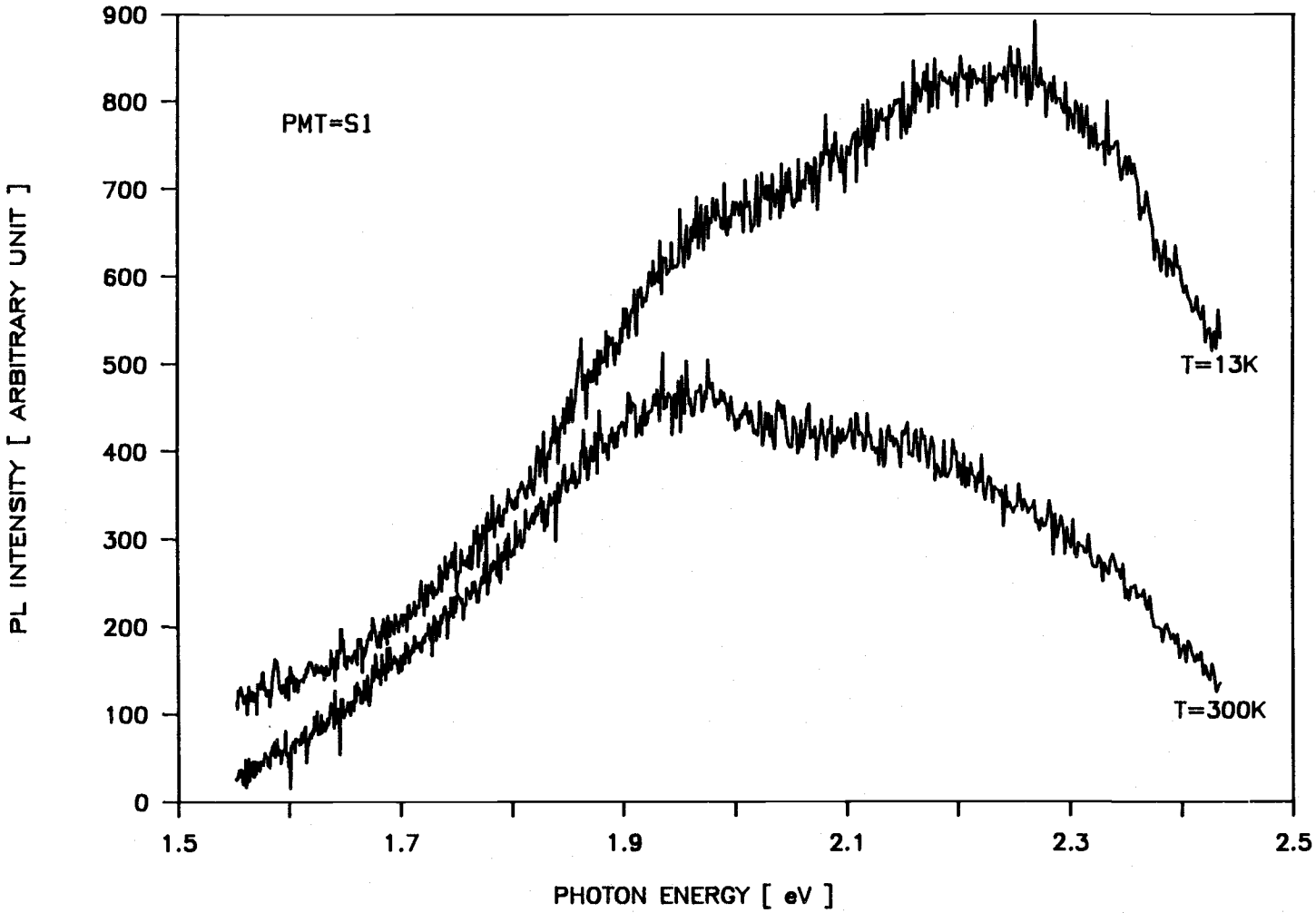

Figure 4.7. PL spectra of HF DLC films measured at 13 K and 300 K.

4.4 Electroluminescence from DLC ACTFEL Devices

Three types of ACTFEL devices using HF DLC films, LF DLC films, and PWRD DLC films as active layers, were fabricated using the deposition parameters shown in Table 3.2 (section 3.5). Measured dielectric constants and breakdown voltages of the ACTFEL device layers are given in Table 4.7.

Table 4.7. Measured dielectric constant and breakdown field of the ACTFEL device layers.

	Material	Dielectric Constant	Breakdown Field
Top insulator	Al_2O_3	~ 14	7.5 MV/cm
Active layer	HF DLC	~ 4	5.1 MV/cm
	LF DLC	~ 4	3.2 MV/cm
	PWRD DLC	~ 4	1.2 MV/cm
Bottom insulator	$Si_xO_yN_z$	~10	7.0 MV/cm

The approximate layer thicknesses of the EL devices fabricated are as follows: 1800 Å for $Si_xO_yN_z$, 1800 Å for DLC, and 2700 Å for Al_2O_3. The top electrode is evaporated Al. The process parameters and physical properties of the three types of DLC films used for EL applications are summarized in Table 4.8. White EL was observed at room temperature from all of the ACTFEL devices when an ac voltage of 200-360 V was applied between the ITO and Al electrodes.

Table 4.8. Summary of the process parameters and physical properties of the three types of DLC films used for ACTFEL fabrication.

Type of DLC film	Temp. (°C)	Power Density (mW/cm^2)	Press. (mT)	Freq. (Hz)	Electrode Spacing (mm)	Relative Mechanical Hardness
HF DLC	50	87	800	13.56 M	16.7	Soft
LF DLC	100	18	950	100 k	50	Hard
PWRD DLC	~250	175	800	13.56 M	34	Inter-mediate

Type of DLC film	Breaking Field * (MV/cm)	Resistivity† (ohm-cm)	E_{opt} (eV)	PL Intensity	Relative PL Peak (eV)	EL Peak (eV)
HF DLC	5.1	$8X10^{14}$	2.5	Bright	2.0,2.2	-
LF DLC	3.2	$4X10^{13}$	1.8,2.4	Dim	1.9,2.15	-
PWRD DLC	1.2	$4X10^{11}$	2.2,2.9	Bright	2.3	1.9

* Field at which a current of 1 μA is measured using an electrode area of $4x10^{-3}$ cm^2 (i.e. at J=0.25 mA/cm^2).

† Resistivity at a field of 1 MV/cm.

The mode of operation of the DLC ACTFEL device is believed to be as follows. When sufficient voltage is applied to the electrodes, electrons are emitted from traps at the negatively biased semiconductor-insulator interface and are accelerated by the field. If an electron gains sufficient kinetic energy during acceleration through the semiconductor, it will have some probability of losing its kinetic energy by electron-hole pair generation. A significant number of these electrons and holes will occupy band tail states while some of the carriers will occupy extended states. Luminescence is obtained through radiative electron-hole recombination via band tail states. When electrons reach the opposite side of the interface, they are trapped in the interface states. The light can be continuously emitted by applying ac electric field between the two electrodes, such that the electrons surge back and forth from one interface to the other.

The luminescence from ACTFEL devices to date has been very dim, observable only in a dark room.

One ACTFEL device was fabricated using the low temperature (50 °C) HF DLC film process procedure. This device was prone to catastrophic breakdown and exhibited a very large EL threshold of 360 V. The spectral response analysis of this device was not accomplished because the luminescence was too dim.

Two ACTFEL devices were fabricated using the LF DLC film process. These devices have a luminescence threshold

voltage of approximately 250 V, but are, to date, not as bright as the PWRD DLC ACTFEL devices fabricated.

One ACTFEL device was fabricated using the PWRD DLC film process. This device is the brightest device to date, and the emission appears yellowish-white. The EL spectrum for this device, and the PL spectrum for a DLC film deposited using the same deposition parameters are compared in Fig. 4.8.

The EL emission intensity peaks at 1.9 eV (red) and extends to 2.4 eV (green). This figure may be misleading, since an S1 photomultiplier tube used for this measurement exhibits a decreasing spectral response with increasing photon energy. The EL peak is located at an energy about 0.4 eV lower than the PL peak. Munekata and Kukimoto have observed [11] the same trend, but to a lesser extent (i.e. 0.2 eV difference), in their a-$Si_{0.3}C_{0.7}$:H ACTFEL devices.

The ac drive voltage (3.5 kHz, 18% duty cycle) and light output voltage waveforms are shown in Fig 4.9. The polarity dependence of the light output waveform is attributed to the asymmetry of the insulators in the MISIM structure.

In contrast to the a-Si_xC_{1-x}:H ac EL device, which emits light only during voltage polarity changes [11], visible light is emitted from the DLC device during virtually the entire duty cycle. The DLC device is similar to the a-Si_xC_{1-x}:H ac EL device, however, in that the decay time of the emission, measured at the trailing edge of the

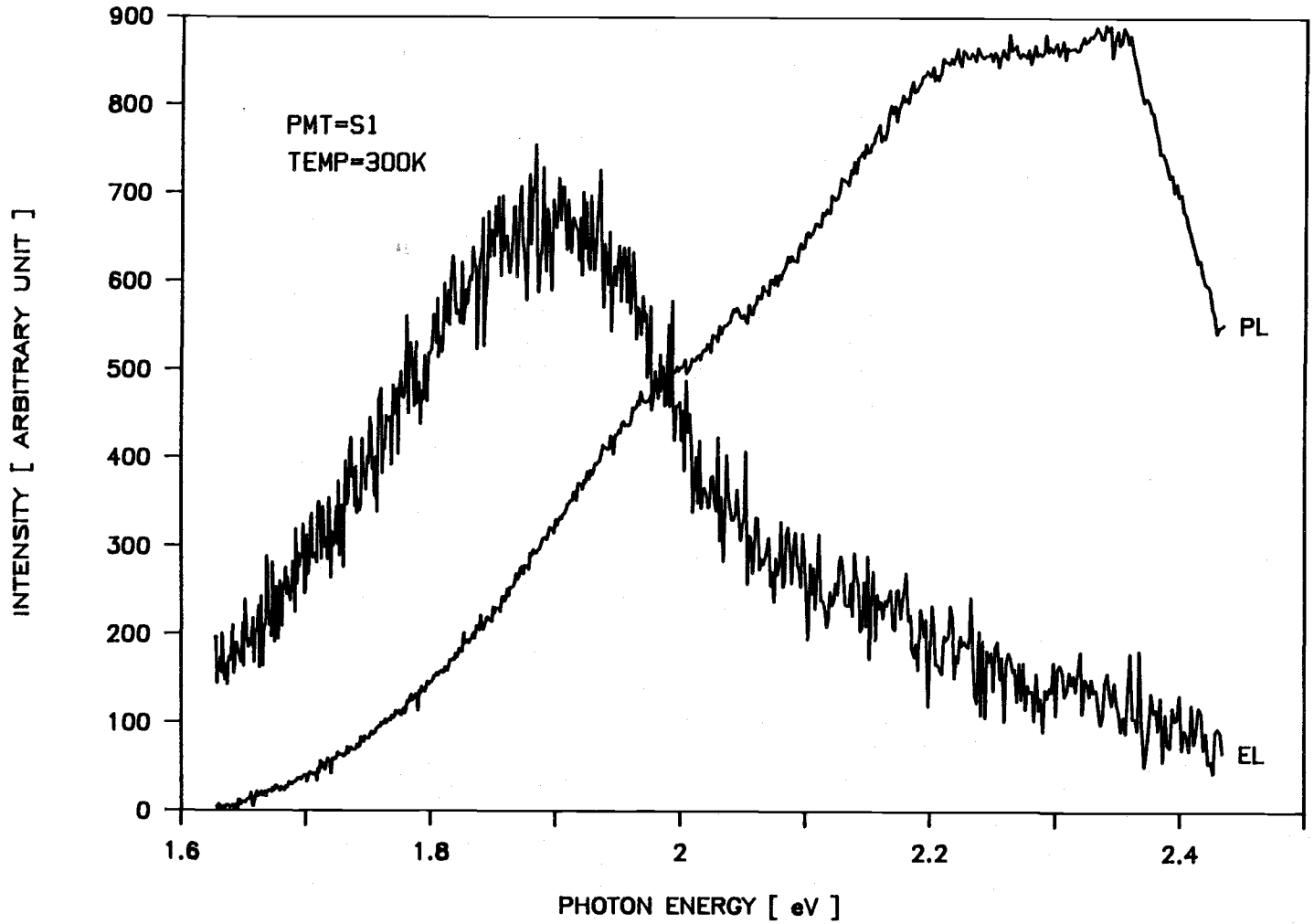

Figure 4.8. EL and PL spectra for the DLC ACTFEL device.

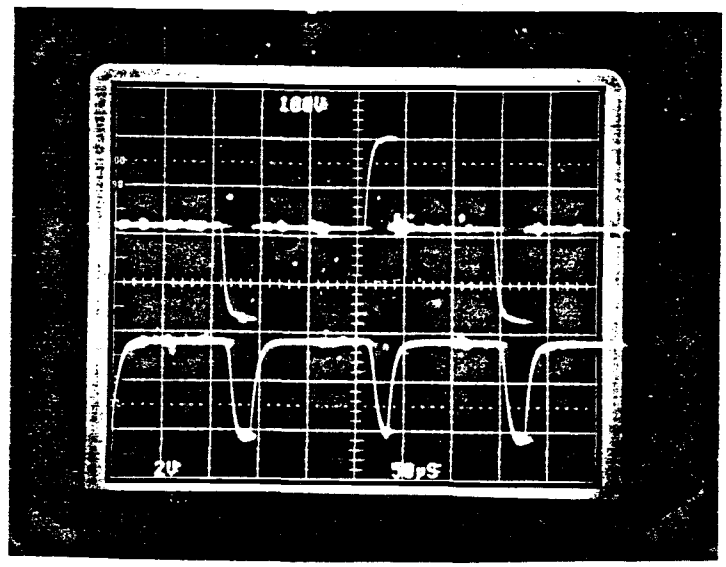

Figure 4.9. AC drive voltage waveform (top) and light output voltage waveform (bottom) for the DLC ACTFEL device.

voltage pulse, is very fast (10 μs), in contrast to that of ZnS:Mn (1 ms) [50].

The brightness-voltage (B-V) and efficiency vs. voltage characteristics of the device are shown in Fig. 4.10 for a 6 kHz ac drive voltage with a 35 % duty cycle. The white EL emission was dim, but observable with the naked eye in a dark room when the drive voltage amplitude exceeded a voltage of 200 V. The threshold voltage was obtained from an extrapolation of the linear portion of Fig. 4.10. Using a dielectric constant value of 4 for DLC, 10 for $Si_xO_yN_z$, and 14 for Al_2O_3, the effective field in the DLC is estimated to

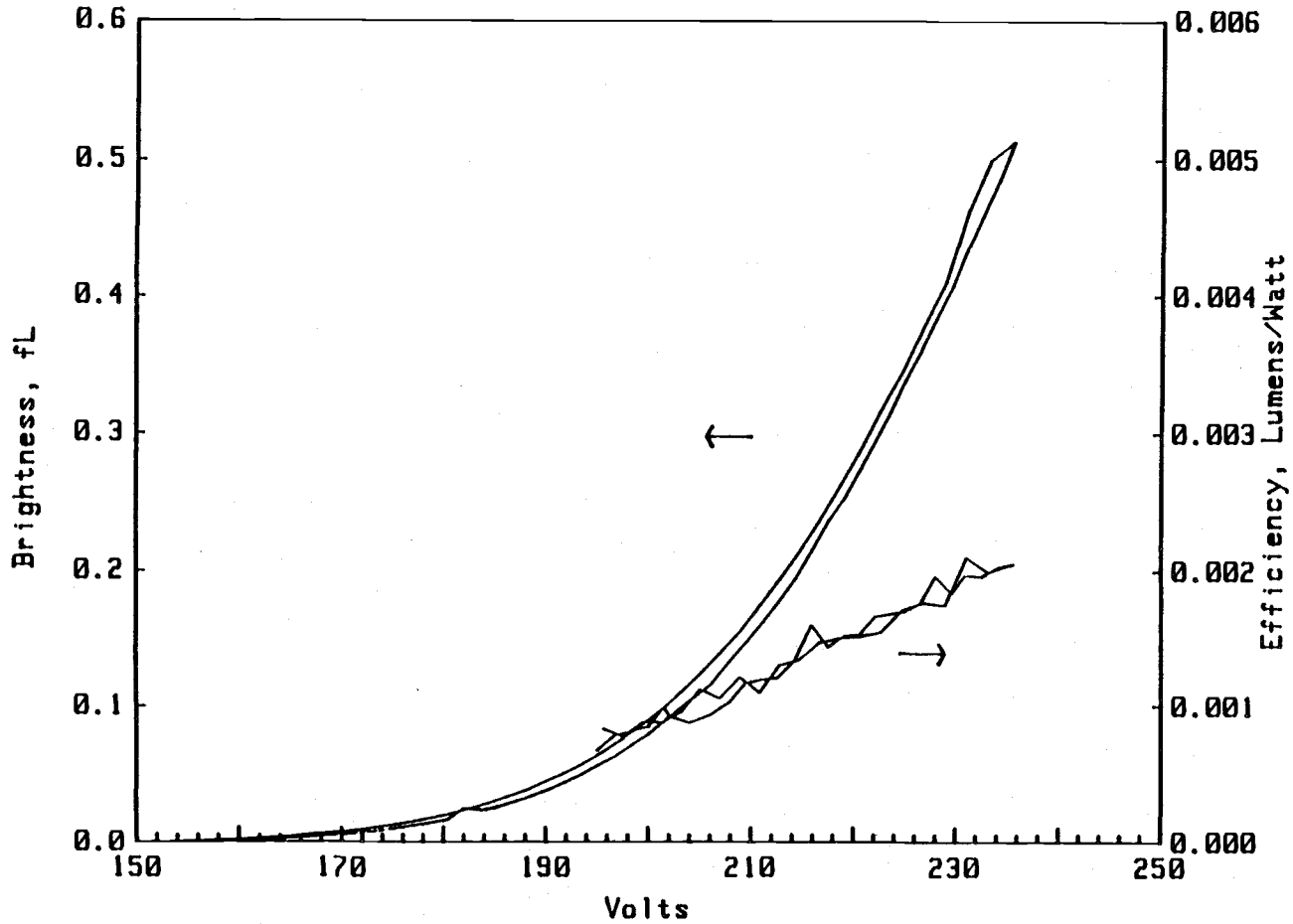

Figure 4.10. Brightness-voltage and efficiency-voltage curves for the DLC ACTFEL device.

be 6 MV/cm at threshold. DLC films deposited in the same manner as for this device exhibited breakdown fields of 1.2 MV/cm (defining breakdown as the field at which a current of 1 uA is measured using an electrode area of 4 x 10^{-3} cm^2, i.e. J = 0.25 mA/cm^2). Thus, this device clearly operates in a breakdown mode. The B-V curve exhibits a small amount of counterclockwise hysteresis. For voltages greater than approximately 210 V the EL efficiency and brightness increase linearly with applied voltage until catastrophic breakdown at approximately 245 V. The brightness and EL efficiency are 0.5 footlamberts (fL) and 0.002 lumens/watt, respectively, at an applied voltage of 235 V. These values are very low at present.

The brightness-frequency (B-F) characteristic is illustrated in Fig. 4.11 for a fixed voltage of 240 V. The brightness increases in almost a linear fashion over the entire range of frequency investigated (up to 6 kHz). To accomplish this measurement, the pulse width was held constant at 30 μs such that an increase in frequency corresponds to an increase in the duty cycle. Preliminary analysis suggests that it is the duty cycle rather than the frequency which leads to the observed increase in brightness. A similar increase in brightness with frequency has been observed [50] in ZnS:Mn devices but the issue of the duty cycle was not discussed.

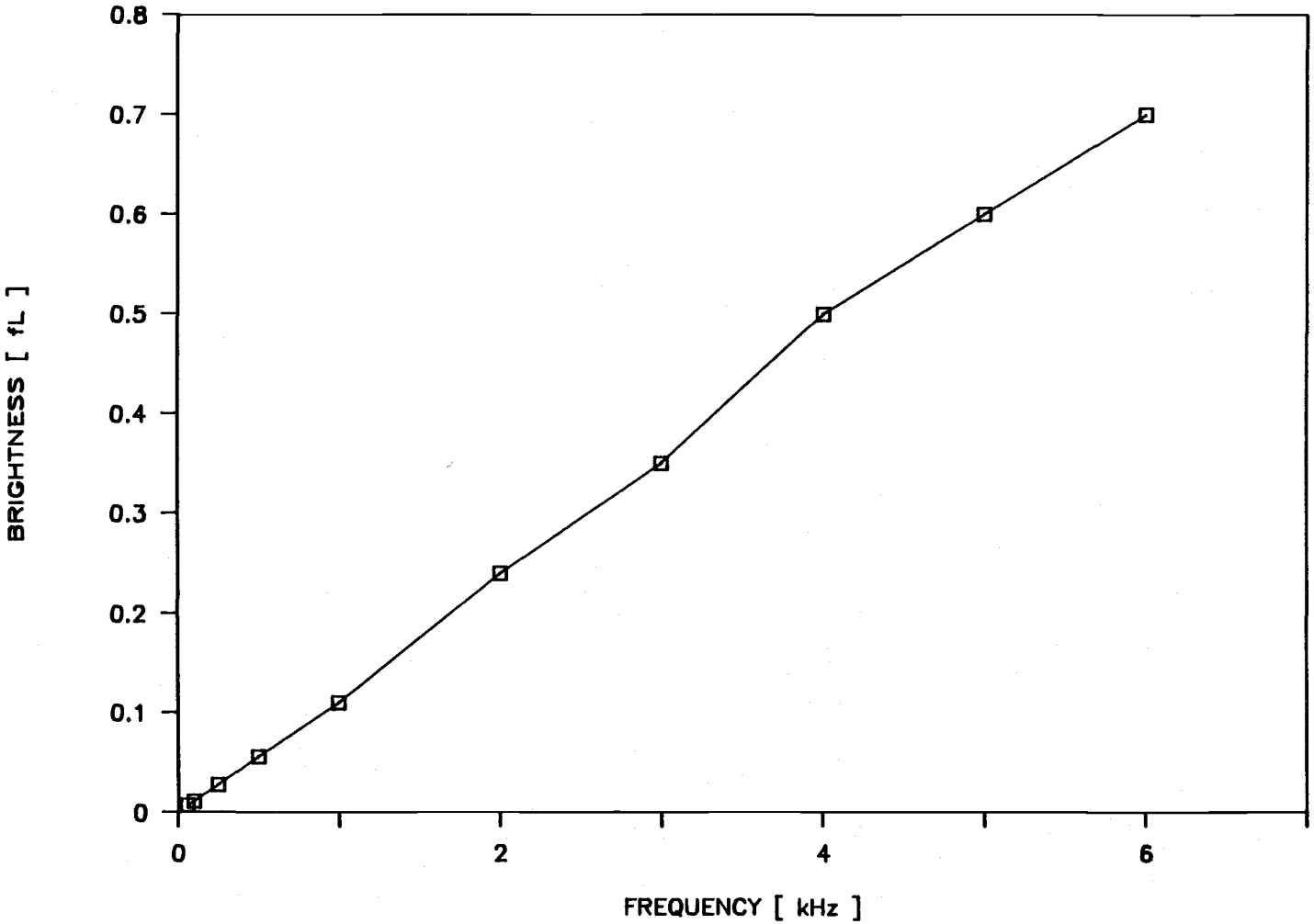

Figure 4.11. Brightness versus frequency plot at a constant voltage of 240 V for the DLC ACTFEL device.

Chapter 5. Conclusions and Recommendations for Future Work

The potential of DLC as an EL material has been experimentally demonstrated by the fabrication of a DLC ACTFEL device which emits broadband, visible EL. Some of the major accomplishments presented in this thesis are:

1. White electroluminescence was observed for the first time from DLC films at room temperature. At an applied voltage of 235 V, the brightness and the efficiency were 0.5 footlamberts (fL) and 0.002 lumens/watt, respectively.

2. The critical temperature for obtaining a DLC deposition was observed to be a function of the electrode spacing. Using the conventional electrode spacing of 25 mm, it was not possible to deposit DLC films above 200 °C. When the electrode spacing was decreased to 14.5-16.7 mm, however, DLC films were obtained at substrate temperatures up to 300 °C.

3. With the modified electrode system, various kinds of DLC films, from soft to hard, were obtained by changing the chamber pressure, in contrast to the HF DLC films deposited by the unmodified electrode system in which the properties were relatively independent of pressure.

4. The optical bandgap, E_{opt} was determined by fitting absorption data to the expression.

$$\alpha h\nu = B\,(h\nu - E_{opt})^2$$

E_{opt} was estimated as 2.2 eV or 2.9 eV from the $(\alpha h\nu)^{\frac{1}{2}}$ vs. $h\nu$ plot (Fig 4.3) for the PWRD DLC films. The PL

spectrum for the sample deposited with the same deposition parameters, however, exhibited a peak at 2.3 eV and a shoulder at 1.95 eV.

5. The PL peak energy was a function of the deposition power. The PL peak energy shifted from 2.1 eV to 1.93 eV with increased deposition power from 30 W to 60 W. Shifts in the PL peak, however, did not occur for DLC films deposited at even higher deposition powers of 80 W-100 W.

6. The PL peak energy increased from 1.93 eV to 2.2 eV with decreased measuring temperature from 300 K to 13 K.

7. Periodic oscillations in the PL spectra of DLC films were observed when the optical pumping energy was decreased from 2.54 eV to 2.41 eV. The period of these oscillations was approximately 0.18 eV, corresponding to C-H wagging-mode energy.

8. The optical bandgap of DLC films deposited by the unmodified electrode structure did not strongly depend on the deposition temperature, RF power, or pressure, in contrast to other reports. This lack of sensitivity was attributed to the use of helium as a diluent gas; the small mass of helium, and its low kinetic energy, minimizes the atomic bombardment damage to the growing film.

9. The optical bandgap of DLC films thermally annealed at 250 °C for 20 minutes decreases by about ΔE_{opt}=0.2-0.5 eV as compared to that of as-deposited DLC films.

10. The refractive index of DLC films obtained ranges from 1.41 to 2.5. DLC films with a higher index of

refraction are harder, but the optical bandgap is smaller.

11. The field strength of DLC films deposited using various deposition parameters is estimated to be above 10^6 V/cm, but to be below 10^6 V/cm for films deposited at high power and low frequency exication.

12. In a comparison of EL and PL spectra, the EL peak energy was about 0.4 eV lower than PL peak energy.

Although a successful ACTFEL device was produced, the luminescent intensity and efficiency of this device is presently very low. There are several tasks to consider for improving the luminescent quality of the DLC films and the device performance:

1. Usage of hydrogen as a diluent gas:

Improvement in the luminescent quality of the DLC film is possible by the addition of hydrogen as a diluent gas. Increasing the partial pressure of hydrogen during the PECVD process will effect a more complete hydrogenation of the DLC film with a concomitant reduction in the spin density which results in larger optical bandgap of the film.

2. Electron spin density measurements:

Further work on DLC films for EL applications should focus on the issue of growing DLC films with a low spin

density, as determined by electron spin resonance (ESR). It has been shown previously [59,60] that a-Si:H and a-Si_xC_{1-x} films which display the most efficient PL properties (under the assumption that efficient PL will translate into efficient EL) also have low ESR spin density. The spin density is related to the density of dangling bonds which is responsible for nonradiative recombination and reduced PL efficiency.

3. PL measurements using a higher optical pumping energy:

Additional work is required to analyze the PL characteristics of the DLC films with higher optical pumping energy. At present our maximum optical pumping energy is 2.54 eV (4880 Å in wavelength). If a higher pumping energy is used, e.g. 4.0 eV, it could be determined whether band states are involved in the radiative transition. If a band is involved, the emission peak of the PL should shift to higher energies.

4. DLC film deposition by a remote PECVD system:

Ion bombardment in the conventional PECVD process results in films with a large density of defects and with correspondingly low PL and EL efficiencies. Advanced plasma processing techniques such as indirect PECVD or electron cyclotron resonance (ECR) plasma deposition can be employed to give DLC films with low spin density. Superior quality films are obtained because the plasma is positioned in a remote location from the substrate which decouples the plasma from the growing film so that the depositing species impinge on the substrate surface with low deposition energies.

5. Band tail engineering:

It is possible that if certain impurities, e.g. nitrogen, were incorporated into the DLC film, the band tail density states could be engineered to give better PL and EL efficiencies.

BIBLIOGRAPHY

[1] D. Theis," Application of Thin Film Electroluminescent Devices," J. Luminescence, Vol. 23, p 191-207, 1981.

[2] S. K. Tiku and G. C. Smith," Choice of Dielectric for TFEL Displays," IEEE Trans. Electron Dev., Vol. ED-31, No. 1, p 105-108, 1984.

[3] R. Wolfe and J. Woods," Electroluminescence of Semiconducting diamond," Phys. Rev. vol.105, No.3, p 921-922, 1957.

[4] J. Walker," Optical Absorption and Luminescence in Diamond," Reports on Prog. Phys., Vol. 42, p 1605-1659, 1979.

[5] J. Levinson and A. Halperrin," The Electro-luminescence(EL) of Natural Semiconducting Diamond," J. Luminescence, Vol. 18/19, p 749-754, 1979.

[6] N. T. Klimenkova, Yu. M. Rotner, E. O. Prokopchuk, V. A. Laptev, V. A Presnov, and V. P. Butuzov," Electro-luminescence of Semiconducting Synthetic Diamonds," Sov. Phys. Semicon., Vol. 11, No. 4, p 361-362, 1977.

[7] A. Lepek and A. Halperin," Electroluminescence (EL) from Natural Semiconducting (p-type) Diamond," J. Luminescence, Vol. 15, p 405-419, 1977.

[8] I. Watanabe, S. Hasegawa, and Y. Kurata," Photo-luminescence of Hydrogenated Amorphous Carbon Films," Jpn. J. Appl. Phys., Pt. 1, Vol. 21, No. 6, p 856-859, 1982.

[9] I. Watanabe and M. Inoue," Photoluminescence in Amorphous C:H Films Prepared by Glow Discharge Decoposition of CH_4 or C_2H_6," Jpn. J. Appl. Phys., Pt. 2, Vol. 22, No. 3, p L176-178, 1983.

[10] I. Watanabe, M. Inoue, and T. Atoji," Photoluminescence in Glow Discharge a-C:H Films," J. Non-Crystalline Solids, Vol. 59/60, p 377-380, 1983.

[11] H. Munekata and H. Kukimoto," Electroluminescence in Hydrogenated Amorphous Silicon-Carbon Alloy," Appl. Phys. Lett., Vol. 42, No. 5, p 432-434, 1983.

[12] D. Kruangam, T. Endo, M. Deguchi, W. Guang-Pu, H. Okamoto, and Y. Hamakawa," Amorphous Silicon-Carbide Thin Film Light Emitting Diode," Optoelectronics, Vol. 1, No.1, p 67-84, 1986.

[13] F. Alvarez, H. L. Fragnito, and I. Chambouleyron," Electroluminescence from Amorphous Silicon Carbide Heterojunctions under Reverse Biased Conditions," J. Appl. Phys. Vol. 63, no. 1, p 244-246, 1987.

[14] J. Robertson," Amorphous Carbon," Adv. in Phys., Vol. 35, No. 4, p 317-374, 1986.

[15] J. C. Angus, P. Koidl, and S. Domitz, in Plasma Deposited Thin Films, Edited by J. Mort and F. Jensen (CRC Press, Boca Raton, FL, 1986).

[16] H. C. Tsai and D. B. Bogy," Critical Review-Characterization of Diamondlike Carbon Films and their Application as Over Coats on Thin-Film Media for Magnetic Recording," J. Vac. Sci. A. Vol. 5, No 6, p 3287-3312, 1987.

[17] J. E. Sundgren and H. T. G. Hentzell," A Review of the Present State of Art in Hard Coatings Grown from the Vapor Phase," J. Vac. Sci. Tech. A., Vol. 4, No. 5, p 2259-2279, 1986.

[18] B. S. Meyerson," Hydrogenated Amorphous Carbon (a-C:H), an Overview," Mat. Res. Soc. Symp. Proc. Vol. 68, p 191-198, 1986.

[19] J. A. Woollam, H. Chang, and V. Natarajan," Diamondlike Carbon: A Bibliography of Published Papers and Reports," Appl. Phys. Comm.,Vol. 5, No. 4, p 263-283, 1985-86.

[20] C. Weissmantel, K. Bewilogua, K. Breuer, D. Dietrich, V. Ebersbach, H.-J. Erler, B. Rau, and G. Reisse," Preparation and properties of Hard i-C and i-BN Coatings," Thin Solid Films, Vol. 96, p 34-44, 1982.

[21] J. C. Angus," Empirical Categorization and Naming of "Diamond-Like" Carbon Films," Thin Solid Films, Vol. 142, p 145-151, 1986.

[22] J. D. Warner, J. J. Pouch, S. A. Alterovitz, and D. C. Liu," Plasma Deposited Hydrogenated Carbon on GaAs and InP," J. Vac. Sci. Tech. A., Vol. 3, No. 3, p 900-903, 1985.

[23] J. D. Lamb and J. A. Woollam," Dielectric Properties of " Diamondlike Carbon " Prepared by r.f. Plasma

Deposition," J. Appl. Phys., Vol. 57, No. 12, p 5420-5423, 1985.

[24] K. Fujii, N. Shohata, M. Mikami, and M. Yonzawa," Properties of Carbon Films by DC Plasma Deposition," Appl. Phys. Lett., Vol. 47, No. 4, p 370-372, 1985.

[25] D. Nir and M. Mirtich," Thin Film Growth Rate Effects for Primary Ion Beam Deposited Diamondlike Carbon Films," J. Vac. Sci. Technol. A, Vol. 4, No. 3, p 560-563, 1986.

[26] S. Aisenberg and R. Chabot," Ion-Beam Deposition of Diamondlike Carbon," J. Appl. Phys., Vol. 42, No. 7, p 2953-2958, 1971.

[27] A. Hiraki, T. Kawano, and Y. Kawakami," Tetrahedral Carbon Film by Hydrogen Gas Reactive RF-Sputtering of Graphite onto Low Temperature Substrate," Solid State Comm., Vol. 50, No. 8, p 713-716, 1984.

[28] O. Matsumoto, H. Toshima, and Y. Kanzaki," Effect of Dilution Gases in Methane on the Deposition of Diamond-like Carbon in a Microwave Discharge," Thin Solid Films, Vol. 128, p 341-351, 1985.

[29] Y. Catherine and P. Couderc," Electrical Characteristics and Growth Kinetics in Discharges Used for Plasma Deposition of Amorphous Carbon," Thin Solid Films, Vol. 144, p 265-280, 1986.

[30] P. Couderc and Y. Catherine," Structure and Physical properties of Plasma-Grown Amorphous Hydrogenated Carbon Films," Thin Solid Films, Vol. 146, p 93-107, 1987.

[31] Shu-Han Lin and B. J. Feldman," Amorphous Hydrogenated Carbon from the Plasma Deposition of C_2H_2, C_2H_4 or CH_4," Phil. Mag. B., Vol. 47, No. 1, p 113-116, 1983.

[32] S. H. Lin and B. J. Feldman," Sidebands in the Luminescence Spectra of Amorphous Hydrogenated Carbon," Phys. Rev. Lett., Vol. 48, No. 12, p 829-831, 1982.

[33] J. Wagner and P. Lautenschlager," Hard Amorphous Carbon Studied by Ellipsometry and Photoluminescence," J. Appl. Phys., Vol. 59, No. 6, p 2044-2047, 1986.

[34] S. Craig and G. L. Harding," Structure, Optical Properties and Decomposition Kinetics of Sputtered Hydrogenated Carbon," Thin Solid Films, Vol. 97, p 345-361, 1982.

[35] S. Kaplan, F. Jansen, and M. Machonkin," Characterization of Amorphous Carbon-Hydrogen Films by Solid-State Nuclear Magnetic Resonance," Appl. Phys. Lett., Vol. 47, No. 7, p 750-753, 1985.

[36] F. W. Smith," Optical Constants of a Hydrogenated Amorphous Carbon Film," J. Appl. Phys., Vol. 55, No. 3, p 764-771, 1984.

[37] M. P. Nadler, T. M. Donovan, and A. K. Green," Thermal Annealing Study of Carbon Films Formed by the Plasma Decomposition of Hydrocarbons," Thin Solid Films, Vol. 116, p 241-247, 1984.

[38] B. Dischler, A. Bubenzer, and P. Koidl," Bonding in Hydrogenated Hard Carbon Studied by Optical Spectroscopy," Solid State Comm., Vol. 48, No. 2, p 105-108, 1983.

[39] J. Fink, Th. Muller-Heinzerling, J. Pfluger, and B. Scheerer," Investigation of Hydrocarbon-Plasma-Generated Carbon Films by Electron-Energy-Loss Spectroscopy," Phys. Rev. B., Vol.30, No. 8, p 4713-4718, 1984.

[40] V. Natarajan, J. D. Lamb, and J. A. Woollam," "Diamondlike" Carbon Films: Optical Absorption, Dielectric Properties, and Hardness Dependence on Deposition Parameters," J. Vac. Sci. Tech. A., Vol. 3, No. 3, p 681-685, 1985.

[41] Ch. Wild and P. Koidle," Thermal Gas Effusion from Hydrogenated Amorphous Carbon Films," Appl. Phys. Lett., Vol. 19, No. 19, p 1506-1508, 1987.

[42] J. A. Reimer and R. W. Vaughan," Proton NMR Studies of Amorphous Plasma-Deposited Films," in Nuclear and Electron Resonance Spectroscopies Applied to Materials Science, edited by E. N. Kaufmann and G. K. Shenoy, Elsevier North Holland, INC, 1981.

[43] N. F. Mott and E. A. Davis, Electronic Processes in Non-Crystalline Materials, 2nd edition, Clarendon Press, Oxford, 1979.

[44] B. Chapman, Glow Discharge Processes, John wiley & Sons, New york, 1980.

[45] J. D. Warner, J. J. Pouch, S. A. Alterovitz, and D. C. Liu," Plasma Deposited Hydrogenated Carbon on GaAs and InP," J. Vac. Sci. Tech. A., Vol. 3, No. 3, p 900-903, 1985.

[46] H. Yasuda and T. Hsu," Plasma Polimerization Investigated by the Comparison of Hydrocarbons and Perfluorocarbons," Surface Science, Vol. 76, p 232-241, 1978.

[47] D. L. Hoffman, N. J. Ianno, and M. A. Mahowald," Plasma Etching of Diamondlike Carbon Films," Appl. Phys. Comm., No. 4, p 203-210, 1985-86.

[48] B. Meyerson and F. W. Smith," Electrical and Optical proper-ties of Hydrogenated Amorphous Carbon Films," J. Non-Crystal-line Solids, Vol. 35/36, p 435-440, 1980.

[49] D. A. Anderson," The Electrical and Optical Properties of Amorphous Carbon Prepared by the Glow Discharge Technique," Phil. Mag. B., Vol. 35, No. 1, p 17-26, 1977.

[50] R. Mach and G. O. Muller," Physical Concepts of High Field, Thin Film Electroluminescent Devices," Phys. Status Solidi a, Vol. 69, p 11-66, 1982.

[51] D. J. Wolford, J. A. Reimer, and B. A. Scott," Efficient Visible Photoluminescence in the Binary a-Si:H_x Alloy System," Appl. Phys. Lett., Vol. 42, No. 4, p 369-371, 1983.

[52] H. Kukimoto, in Semiconductors and Semimetals, Vol. 21D, edited by J. I. Pancove, (Academic, Orlando, FL, 1984), p 239.